Future methane, hydroxyl, and their uncertainties: key climate and emission parameters for future predictions

Christopher D. Holmes [1*], Michael J. Prather [1], Amund O. Søvde [2], Gunnar Myhre [2]

[1] Department of Earth System Science, University of California, Irvine, CA 92697-3100 USA

[2] Center for International Climate and Environmental Research (CICERO), Oslo, Norway

[*] Correspondence to cdholmes@uci.edu

Abstract

Accurate prediction of future methane abundances following a climate scenario requires understanding the lifetime changes driven by anthropogenic emissions, meteorological factors, and chemistry-climate feedbacks. Uncertainty in any of these influences or the underlying processes implies uncertainty in future abundance and radiative forcing. We simulate methane lifetime in multiple models over the period 1997-2009, adding sensitivity tests to determine key variables that drive the year-to-year variability. Across three atmospheric chemistry and transport models—UCI CTM, GEOS-Chem, and Oslo CTM3—we find that temperature, water vapor, ozone column, biomass burning and lightning NOx are the dominant sources of interannual changes in methane lifetime. We also evaluate the model responses to forcings that have impacts on decadal time scales, such as methane feedback, and anthropogenic NOx emissions. In general, these different CTMs show similar sensitivities to the driving variables. We construct a parametric model that reproduces most of the interannual variability of each CTM and use it to predict methane lifetime from 1980 through 2100 following a specified emissions and climate scenario (RCP 8.5). The parametric model propagates uncertainties through all steps and provides a foundation for predicting methane abundances in any climate scenario. Our sensitivity tests also enable a new estimate of the methane global warming potential (GWP), accounting for stratospheric ozone effects, including those mediated by water vapor. We estimate the 100-year GWP to be 32.

1 Introduction

Rising atmospheric concentrations of greenhouse gases are the main cause of current and future climate change (Intergovernmental Panel on Climate change IPCC, 2007). Uncertainty in mapping an emission scenario onto future abundance of greenhouse gases (GHGs) thus translates almost directly into uncertainty in our ability to project climate change and its impact on nature and society. To date, IPCC has generally adopted a single trajectory for the growth of greenhouse gases in each of several different socio-economic scenarios, thus neglecting uncertainty in those future abundances. For methane, the second most important anthropogenic GHG, these trajectories are based on simple parametric formulas for methane lifetime. In the IPCC Third Assessment Report (TAR), 4 parameters accounted for the change in tropospheric OH, the largest atmospheric methane sink, due to anthropogenic emissions of CO, nitrogen oxides (NOx), and volatile organic compounds (VOCs) and the negative feedback between methane abundance and tropospheric OH (Prather et al., 2001). Other sinks, which include oxidation in the stratosphere, oxidation by tropospheric chlorine, and uptake into soil, were assessed but assumed not to change during the 21st century projections. For the upcoming IPCC 5th Assessment Report (AR5) the Representative Concentration Pathway (RCP) scenarios adopt methane trajectories calculated in the MAGICC model, which augments the TAR parametric formula with a temperature term (Meinshausen et al., 2011a).

On small spatial scales, OH concentrations and methane oxidation depend on temperature, pressure, sun elevation, clouds, UV attenuation by stratospheric ozone, and local concentrations of water vapor, ozone, CH_4, CO, NOx, VOCs, and aerosols (e.g. Duncan et al., 2000; Olson et al., 2006). Integrated globally and annually, some of these influences are small, but numerous studies have found that temperature, circulation, water vapor, stratospheric ozone, clouds and natural and anthropogenic emissions are important (Dentener et al., 2003; Fiore et al., 2008a; Hess and Mahowald, 2009; Lelieveld and Crutzen, 1994; Stevenson et al., 2005; Voulgarakis et al., 2010). Uncertainties in these factors and in the present-day methane budget mean that each socioeconomic emission scenario could produce a range of future methane abundances (Prather et al., 2012).

Global climate model (GCM) simulations with atmospheric chemistry provide another method for predicting future methane and other chemically reactive GHGs. An ensemble of such models can provide a range of future methane abundances for a single scenario (e.g. Atmospheric Chemistry and Climate Model Intercomparison Project (ACCMIP) Lamarque et al., n.d.),

spanning some, but likely not all, future uncertainties. This approach is computationally expensive, however, which restricts the number of socioeconomic scenarios and ensemble members that can be explored.

In this work we develop a new parametric model for global methane lifetime that accounts for climate-chemistry interactions that were neglected in previous approaches. We derive the parametric factors from perturbation tests in a suite of 3 chemical transport models (CTMs), since CTMs with detailed tropospheric chemistry provide the best mechanistic representation of methane loss from tropospheric OH. We focus on the tropospheric OH sink because other methane sinks are smaller and their intrinsic variability has a smaller impact on the total methane lifetime. The parametric model accounts for uncertainty in atmospheric chemistry based on the range of perturbation responses across the CTMs. The perturbation tests also enable a new estimate of the ozone contribution to methane radiative forcing and global warming potential. We evaluate the parametric model against 13-year CTM simulations of methane lifetime, and against observed variability in tropospheric OH, as measured by the decay of methyl chloroform. Finally, we use this parametric model with uncertainties to make new projections of methane and its uncertainties through 2100.

2 Model descriptions

We diagnose methane lifetime due to tropospheric OH, $\tau_{CH4\times OH}$, from multi-year simulations in 3 different CTMs: University of Oslo CTM3, University of California, Irvine (UCI) CTM, and GEOS-Chem. All of these models are driven by assimilated meteorological data and configured to use the same emissions from anthropogenic, biogenic and biomass burning sources. We use year-specific meteorology spanning 1997-2009 for each model, except GEOS-Chem simulations with GEOS-5 meteorology, which are only 2004-9 (see below). Subsections 2.1-2.4 summarize unique features of each model and describe the emissions.

Monthly chemistry diagnostics from each model enable us to calculate $\tau_{CH4\times OH}$, defined as the total atmospheric CH_4 burden divided by its loss through reactions with tropospheric OH. All 3 models use fixed methane abundances (1760 ppb for UCI CTM and CTM3, 1775 ppb for GEOS-Chem), so variations in $\tau_{CH4\times OH}$ are due solely to changes in the OH sink. Different tropopause definitions in the models have minimal effect on $\tau_{CH4\times OH}$ since CH_4 oxidation between 200 hPa and the tropopause is 1.5% of tropospheric methane loss, or less. We calculate the total methane lifetime, τ_{CH4}, using $\tau_{CH4\times OH}$ values from this work and recently estimated lifetimes for other

methane sinks: tropospheric chlorine (200 y), stratosphere (120 y), and soil (150 y) (Prather et al., 2012).

2.1 Oslo CTM3

Oslo CTM3 is a stratospheric and tropospheric CTM, recently described by Søvde et al. (2012). Transport is driven by pieced-forecast meteorology from the European Center for Medium-range Weather Forecasting (ECMWF) Integrated Forecast System (cycle 36r1, http://www.ecmwf.int/research/ifsdocs/CY36r1/index.html). The original T359 (~0.55°×0.55°) horizontal resolution and 60 layer vertical resolution of the forecast model is degraded to T42 (~2.8°×2.8°) resolution, while preserving the 3 h temporal resolution for all meteorological fields. Advection uses the second-order moments scheme (Prather, 1986; Prather et al., 2008) and convection follows Tiedtke (1989).

The CTM3 chemical mechanism includes a full stratospheric chemical mechanism in addition to tropospheric reactions. The tropospheric module contains 105 reactions and 51 gas-phase species, including sulfate, nitrate, and sea-salt aerosols. Nitrate aerosols affect the gas-phase chemistry through HNO_3 uptake, which is a sink for reactive nitrogen through subsequent wet scavenging. Photolysis rates required in the chemistry mechanism are calculated online using the Fast-JX method (Neu et al., 2007), with cloud distributions from ECMWF meteorology. CTM3 shares the same chemical mechanism and some other physical process algorithms with the older CTM2, which has been extensively used for studies of present and future tropospheric composition (Dalsoren et al., 2010; Hoor et al., 2009; Isaksen et al., 2005).

2.2 UCI CTM

The UCI CTM is a tropospheric CTM, using the same meteorology, transport algorithms, and Fast-JX photolysis as CTM3. Like CTM3, the UCI CTM uses T42 horizontal resolution, but the vertical resolution in the boundary layer is reduced, so there are 57 layers total. Tropospheric chemistry of the major gas-phase species involved in HOx, NOx, O_3, and VOC reactions is simulated with the ASAD package (Carver et al., 1997), with updates to the mechanism and kinetics (Tang and Prather, 2010). This mechanism includes 84 reactions involving 33 species, making it simpler than the CTM3 chemical mechanism. Simplified stratospheric O_3 chemistry is simulated with Linoz (version 2 Hsu and Prather, 2009). Aerosol effects on photolysis and chemistry are neglected, which increases OH and biases $\tau_{CH4\times OH}$ high by about 10% (Bian et al., 2003; Macintyre and Evans, 2010; Martin et al., 2003).

2.3 GEOS-Chem

GEOS-Chem is a tropospheric CTM, driven by assimilated meteorological data from the NASA Goddard Earth Observing System (GEOS-5) or MERRA reanalysis (Rienecker et al., 2011; 2008). Both GEOS-5 and MERRA are produced from closely related assimilation systems, using the same spatial resolution of 0.5°×0.66° and 72 vertical layers. Most GEOS-Chem results here, including all sensitivity simulations, are based on GEOS-5 meteorology, which has been degraded to 2°×2.5° and 47 layers for the CTM. GEOS-5 data are available only after 2004, however, so we also simulate 1997-2009 using MERRA meteorology at 4°×5° and 47 layers. Temporal resolution in GEOS-5 (MERRA) is 6 h (3 h) for most meteorological quantities and 3 h (1 h) for surface quantities and mixing depth.

The tropospheric chemistry mechanism in GEOS-Chem consists of 104 species and 236 chemical reactions that simulate aerosols in addition to the HOx-NOx-VOC-ozone system, and has recently been updated by Mao et al. (2010). Photolysis rates are calculated with the Fast-JX method, using aerosol optical depths that are simulated internally, and ozone columns from the TOMS and SBUV satellites (until 2008) or GEOS-5 assimilation of satellite data (after 2008). For purposes of stratosphere-troposphere exchange, stratospheric ozone is simulated with Linoz.

2.4 Emissions

Emissions used in this work are representative of 1997-2010, but do not resolve trends or interannual variability in anthropogenic or biogenic emissions. To the extent possible, we use identical emissions across all models. Anthropogenic, biogenic, and biomass burning emissions of NOx, CO, and isoprene are fully consistent in all models. Some differences in VOC emissions arise because of the different lumping schemes used in the various chemical mechanisms and because some VOC species are not simulated in all models. Lightning NOx emissions also differ between models because they are calculated from underlying meteorology, as described below.

Table 1 summarizes emissions of key species. We use the RCP inventory for anthropogenic emissions for year 2000, repeating in each simulated year (Lamarque et al., 2011). This inventory provides monthly gridded emissions for NOx, CO and speciated VOCs from 11 emission activities. Aviation and shipping emissions change each month, while other anthropogenic emission activities are constant throughout the year. Biomass burning emissions are specified for each year and month by the GFED inventory (version 3 van der Werf et al., 2010). We use this instead of the climatological biomass burning emissions provided in the RCP inventory because fires are a major cause of year-to-year variability in tropospheric OH. Biogenic emissions of

isoprene, CO, and other VOCs are from a MEGAN climatology for the 2000s decade (Guenther et al., 2006). GEOS-Chem includes additional oceanic emissions of acetone (13 Tg/a Jacob et al., 2002) and acetaldehyde (57 Tg/a Millet et al., 2010), which are not included in other models. All emission data are provided at 0.5° × 0.5° resolution.

Lightning NOx emissions (L-NOx) are calculated with similar methods in all 3 CTMs, with UCI CTM and CTM3 using identical algorithms. In all models, these emissions are derived from cloud-top heights in the underlying meteorology (Price and Rind, 1994) and scaled to match satellite-observed lightning flash rates (Christian et al., 2003). In the UCI CTM and CTM3, 2 scale factors are calculated to match observed multi-year mean flash rates over land and ocean. In GEOS-Chem scale factors are calculated for every grid column and month (Sauvage et al., 2007). Within the convective column, L-NOx is distributed vertically based on observed NOx distributions (Ott et al., 2010). Søvde et al. (2012) provide a full description of lightning emissions in UCI CTM and CTM3, and Murray et al. (Murray et al., n.d.) do the same for GEOS-Chem. L-NOx averages 6 Tg(N) a^{-1} in GEOS-Chem and 5 Tg(N) a^{-1} in UCI CTM and CTM3.

3 Recent (1997-2009) variability of CH_4 lifetime

Figure 1 shows $\tau_{CH4\times OH}$ for 1997-2009, as simulated by the 3 CTMs. The tropospheric OH lifetimes range from 8.5 to 10.1 years. The longest of these lifetimes (GEOS-Chem) is consistent with the constraint provided by methyl chloroform observations, 11.2 ± 1.3 y (Prather et al., 2012), but all are within the range of contemporary tropospheric chemistry models (e.g. 9.5 ± 1.1 y from ACCMIP Naik et al., n.d.).

These simulations show similar variability of $\tau_{CH4\times OH}$ in all CTMs. Common features include a sharp dip in 1998 and peak in 2000, coincident with a strong El Niño and La Niña, smaller peaks in 2004 and 2008, and general decline after 2005. These features appear robust against the various choices of chemical mechanism, meteorology, and resolution used in these CTMs. In independent work, the ECHAM model also simulates the same features, using different emissions and chemistry (Montzka et al., 2011).

3.1 Methane lifetime sensitivity to chemistry-climate factors

Having identified robust variations in $\tau_{CH4\times OH}$ across multiple CTMs, we examine their causes with explicit perturbation tests. In these tests, we perturb a single climate or emission variable, simulate 3 or more years, discard the first year as spinup, and analyze the difference from the unperturbed simulation in the remaining years. Perturbations are applied to 1997-9 for Oslo

184 CTM3 and the UCI CTM, and to 2004-6 for GEOS-Chem with GEOS-5 meteorology. The
185 sensitivity, α, of $\tau_{CH4\times OH}$ to a climate or emission variable, F, is always defined as $\alpha = d$
186 $\ln(\tau_{CH4\times OH})/d \ln(F)$. As such, α can be interpreted as the percent change in $\tau_{CH4\times OH}$ resulting from a
187 1% increase in F.

188 Table 2 reports sensitivities for the evaluated climate and emission variables. These variables
189 include most of those identified in the literature as important influences on tropospheric OH and
190 $\tau_{CH4\times OH}$: temperature, water vapor, ozone column, convective fluxes, cloud optical depth, biomass
191 burning emissions, and NOx emissions. Perturbation magnitudes are chosen to be similar to the
192 interannual variability or decadal trend of each variable (exact magnitudes in Table S1).

193 Only variables with large sensitivity, large interannual changes, or both can explain the year-to-
194 year $\tau_{CH4\times OH}$ variations identified in Figure 1. Figure 2 shows the interannual changes of 5 key
195 variables for 1997-2009. Water vapor, having about 3% variation and $\tau_{CH4\times OH}$ sensitivity near –
196 0.3, could account for about 1 % interannual variability in $\tau_{CH4\times OH}$. Temperature, ozone column,
197 L-NOx, and biomass burning also have sufficient sensitivity and variability to account for about 1
198 % variation in $\tau_{CH4\times OH}$ over the 1997-2009 period. These 5 climate and emission variables we
199 identify as important influences on $\tau_{CH4\times OH}$ have been recognized previously, but their
200 sensitivities have not been quantified in a comparable way (e.g. Dentener et al., 2003; Fiore et al.,
201 2006; Hess and Mahowald, 2009; Stevenson et al., 2005).

202 Convective fluxes and cloud optical depths for water and ice clouds, as diagnosed in ECMWF
203 meteorology, vary annually by 2 % and have small sensitivity, so these factors have very little
204 impact on $\tau_{CH4\times OH}$. Due to the small impact in the UCI CTM, these perturbation tests are not
205 repeated in the other CTMs. Our results are consistent with the known decrease in mass-weighted
206 global OH concentrations due to clouds (Voulgarakis et al., 2010) because mass-weighted
207 averaging emphasizes below-cloud OH concentrations and we find compensating increases in
208 methane loss above clouds. In addition, past analyses of convective fluxes have found both
209 positive and negative influences on $\tau_{CH4\times OH}$ depending on the convection scheme and perturbation
210 used (Lawrence and Salzmann, 2008).

211 Methane abundance and anthropogenic NOx emissions increased over the 2000-2010 decade by
212 by 1 % and 2 %, respectively, and vary smoothly between years (Dlugokencky et al., 2011;
213 Granier et al., 2011). Therefore, these factors have little impact on $\tau_{CH4\times OH}$ variability during the
214 13-year CTM simulation, but are important on multi-decadal time scales and longer.

Many of the sensitivity terms in Table 2—specifically, water vapor, biomass burning, CH_4 abundance, and anthropogenic land NOx—are consistent among the CTMs and with past estimates (Fiore et al., 2008b; Hoor et al., 2009; Myhre et al., 2011; Prather et al., 2001), suggesting a good understanding of how these variables impact tropospheric methane loss. Adopted values for each sensitivity (Table 2, right column), which are used in the parametric model described below, reflect the consistency among models. For biomass burning, the agreement between models masks large changes in sensitivity between years, shown in Figure 3 for the UCI CTM. The sensitivity is highly correlated with total biomass burning emissions, and the CO/NO ratio in those emissions, both of which suppress tropospheric OH (Duncan et al., 2003; Voulgarakis et al., 2010) and peak during El Niño years due to tropical peat fires. Future climate may be more El Niño-like due to GHG warming (Yamaguchi and Noda, 2006), so, despite the CTM consensus on present-day biomass burning sensitivity, we adopt a broad uncertainty range for future sensitivity.

Other sensitivities, chiefly air temperature and ship NOx, differ by 50% or more across the models. These differences are understandable, however, as consequences of modeling assumptions. For ship NOx, CTM3 and UCI CTM are nearly 3 times more sensitive than GEOS-Chem. In the UCI CTM and CTM3, ship NOx is emitted as NO, diluted into the grid volume, and the subsequent production of O_3 and HNO_3 are calculated by the grid-resolved chemistry. Instantaneous dilution overestimates the NOx lifetime and O_3 production from ships (Chen et al., 2005), however. To compensate, GEOS-Chem instantaneously converts all ship NOx emissions to O_3 and HNO_3, following observed production ratios. As a result, GEOS-Chem underestimates the large-scale impact of shipping, since, in reality, 20-50% of NOx remains after 5 hours following emission (Vinken et al., 2011). Although previous estimates of ship NOx are close to the high values in this work (Hoor et al., 2009; Myhre et al., 2011), the actual atmospheric sensitivity to ship NOx, likely lies somewhere between the GEOS-Chem and UCI CTM results.

Ship NOx emissions also explain the divergence of GEOS-Chem and the UCI CTM in their temperature sensitivities. Over land, both models predict similar reduction $\tau_{CH4\times OH}$ in response to warming. Over the oceans, however, GEOS-Chem predicts longer $\tau_{CH4\times OH}$ at higher temperatures while the UCI CTM predicts the opposite. In the presence of ship NOx in the UCI CTM, higher temperatures increase both the production and loss of O_3, with net excess production; OH rises in turn. In GEOS-Chem, by contrast, higher temperatures increase O_3 destruction over the ocean with less opportunity for enhanced production; OH thus decreases over oceans.

The sensitivity of $\tau_{CH4\times OH}$ to methane abundance is closely related to the methane feedback factor, *f*, which is the ratio of methane perturbation lifetime to total budget lifetime (Prather et al., 2001). Our multi-model mean sensitivity, 0.31 ± 0.04, is similar to past estimates (Fiore et al., 2009; Prather et al., 2001), but we derive a smaller feedback factor $f = 1.34 \pm 0.06$ than has been recommended by IPCC (f = 1.4 Prather et al., 2001) because we use updated estimates of methane lifetime (Prather et al., 2012). Reducing the feedback factor, which was already suggested by Fiore et al. (2009), lowers the methane radiative forcing and global warming potential, as discussed in section 3.5.

3.2 A parametric model for $\tau_{CH4\times OH}$

The sensitivity parameters in Table 2, together with the time series of corresponding climate and emission variables in Figure 2, enable us to build a parametric model for methane lifetime representing each CTM. We combine terms linearly, so that $\tau_{CH4\times OH}$ is approximated by

$$\ln(\tau_{CH4\times OH}(t)) = \ln(<\tau_{CH4\times OH}>) + \Sigma_i \alpha_i \Delta\ln(F_i(t)), \quad (1)$$

where $F_i(t)$ is the time series of forcing variable *i* and $<\tau_{CH4\times OH}>$ is the mean lifetime in the CTM. Figure 1 shows the parametric model reconstruction of each CTM, alongside the actual calculated $\tau_{CH4\times OH}$. We find that 5 variables—temperature, water vapor, column ozone, biomass burning emissions, and L-NOx emissions—explain 90% of the interannual variation in $\tau_{CH4\times OH}$ in the UCI CTM and GEOS-Chem over the simulated period 1997-2009. Even though the GEOS-Chem sensitivity parameters were derived from 2°×2.5° simulations driven by GEOS-5, the 5-parameter model performs equally well compared to the 4°×5° GEOS-Chem simulation driven by MERRA. The sensitivity parameters are thus robust across changes in model resolution and meteorology. For Oslo CTM3 the 5-parameter model explains 50% of $\tau_{CH4\times OH}$ variability overall, rising to 75% outside the 1997-8 ENSO. A higher temperature sensitivity, similar to the UCI CTM, in the parametric model also increases the explained variance for CTM3 to 80%.

The atmospheric chemistry of tropospheric OH and methane involves nonlinear chemistry that could, in principle, undermine the additivity of terms in Equation 1. We test the linearity of the system with a final perturbation test in the UCI CTM in which all 5 factors are perturbed simultaneously. The resulting change in $\tau_{CH4\times OH}$ differs by about 1 part in 10 from the linear addition of factors.

The CTM simulations in this work make several assumptions to simplify the perturbation analysis and enable comparisons between CTMs, but these could alter $\tau_{CH4\times OH}$. In particular, the

simulations neglect variability in biogenic VOC emissions (Guenther et al., 2006), trends in anthropogenic emissions and their location, and trends in atmospheric methane. We compare our GEOS-Chem/MERRA simulation to one that includes all these processes, and other minor model updates, and find correlations of 98% for $\tau_{CH4\times OH}$ (M. Mu, personal communication). Thus, the neglected processes make small to interannual variability of $\tau_{CH4\times OH}$ and do not degrade the parametric model performance.

3.3 Methyl chloroform comparison

Two global measurement networks have recorded the growth and decline of atmospheric methyl chloroform (MCF) since the 1970s (ALE/GAGE/AGAGE Prinn et al., 2005), with expanded coverage since the 1990s (NOAA Montzka et al., 2011). Like methane, atmospheric MCF is oxidized mainly by tropospheric OH, with small additional sinks in the stratosphere, oceans, and soil (Volk et al., 1997; Wang et al., 2008; Wennberg et al., 2004). Because MCF has no natural sources and the anthropogenic production is well known (McCulloch et al., 1999), MCF provides the best available constraint on global OH levels and methane lifetime. The analysis here uses observations since 1998, when anthropogenic MCF emissions became small compared to atmospheric oxidation of the residual atmospheric burden. Consequently, MCF atmospheric lifetimes can be inferred from observed decay rates without detailed accounting for emissions and transport (Montzka et al., 2011).

For each network, we calculate decay rates of MCF from monthly average concentrations provided by each network (NOAA: ftp://ftp.cmdl.noaa.gov/hats/solvents/CH3CCl3/flasks/GCMS/CH3CCl3_MS2011a.txt, accessed Jan 5, 2012; AGAGE: http://agage.eas.gatech.edu/data_archive/agage/gc-md/monthly/, accessed April 4, 2012). For site i and month t the observed decay rate (a^{-1}) is

$$k_{i,t} = -\ln(c_{i,(t+6)} / c_{i,(t-6)}), \quad (2)$$

where $c_{i,t}$ is the concentration at site i in month t. The global MCF decay rate is the average of $k_{i,t}$ across sites within a network. We calculate uncertainty in the global decay rate as the 16^{th}-84^{th} percentile range (i.e. $\pm 1\ \sigma$) of $k_{i,t}$ across sites within a network. No filling is used for months with missing data. (See Supplement for additional method details.) Over 1998-2007, the global MCF decay rates from the 2 networks differ by less than 1% (0.1811 a^{-1} for NOAA, 0.1796 a^{-1} for AGAGE). This analysis, however, focuses on anomalies in the global decay rate, relative to each network's own mean. Because the anomalies are attributed solely to tropospheric OH loss (see

309 below) and for comparison to $\tau_{CH4\times OH}$, to the decay anomalies are divided by $r = 0.87$ to account
310 for the tropospheric OH fraction of total MCF loss (Prather et al., 2012).

311 Figure 4 compares the interannual variability of simulated $\tau_{CH4\times OH}$ in the CTMs against the MCF
312 decay rate. While the CTMs are consistently within the observational uncertainty for both
313 observation networks, the year-to-year changes in the models generally do not correlate with the
314 MCF data. In addition, simulated $\tau_{CH4\times OH}$ in all CTMs varies less than the MCF constraint (1 %
315 vs. 2.3% for σ/mean). Residual anthropogenic or ocean emissions could account for some MCF
316 decay rate anomalies, but only if these emissions change abruptly from year to year. Emission
317 anomalies of about 4 Gg a^{-1} would be required to cause the observed decay rate swings during
318 2002-4. Meanwhile, total anthropogenic and ocean emissions for those years are estimated to be 6
319 and 4 Gg a^{-1}, respectively, and decreasing smoothly (Montzka et al., 2011; Prinn et al., 2005;
320 Wennberg et al., 2004). Therefore, abrupt emission changes might explain part, perhaps half, of
321 the decay anomalies, but cannot account for the full discrepancy between simulated $\tau_{CH4\times OH}$ and
322 observations.

323 Collocated measurement sites in the NOAA and AGAGE networks provide an alternative means
324 to evaluate possible errors in decay rates. At all 4 collocated sites (Cape Grim, American Samoa,
325 Trinidad Head, and Mace Head) we find differences between the networks as large as 2% in the
326 monthly means. (See Figure S2.) The differences exceed the standard error in monthly mean and
327 persist for several consecutive months; thus they are likely not caused by synoptic variability and
328 differences in sampling frequency. Because the biases change over time, they lead to differences
329 of up to 4% in MCF decay rates at a single site. As can be seen in Figure 2, both networks find
330 similar magnitude of OH variability, but they differ in sign and magnitude of the anomaly at
331 many times. Given that differences in observed MCF decay rates between the two networks are as
332 large as their difference from CTM $\tau_{CH4\times OH}$ anomalies, we conclude that better understanding of
333 the systematic differences between the observation networks is required before using them as a
334 constraint on $\tau_{CH4\times OH}$ and OH interannual variability.

335 ## 3.4 Methane global warming potential

336 Global Warming Potentials (GWP) are useful for comparing the radiative forcing (RF) caused by
337 emissions of various GHGs having different absorbances and atmospheric lifetimes. The methane
338 GWP customarily accounts for the direct RF from the emitted gas, as well as indirect RF caused
339 by methane-induced increases in ozone, stratospheric water vapor, and feedback on the methane
340 lifetime (Forster et al., 2007). Here we evaluate the methane GWP implied by the perturbation

experiments. Radiative forcing of methane and ozone are calculated for the control simulation and a simulation with 5% more methane, using the University of Oslo radiative transfer model (Myhre et al., 2011). In addition, we test the effect of methane-induced water vapor on stratospheric ozone, with an additional Oslo CTM3 simulation in which stratospheric water vapor was increased to maintain equilibrium with the CH_4 perturbation. To our knowledge, this indirect, H_2O-mediated effect on ozone has not been included in prior assessments of methane GWP.

Table 5 summarizes ozone changes and RF results for all simulations, normalized to 1 ppb CH_4 perturbations. Tropospheric ozone changes in GEOS-Chem and the UCI CTM (2.9 and 4.0 DU ppm$(CH_4)^{-1}$, respectively) are within the range of previous multi-model studies (Fry et al., 2012; Holmes et al., 2011). Oslo CTM3, however, exhibits larger tropospheric changes (5.0 DU ppm$(CH_4)^{-1}$), likely due to the effects of stratospheric chemistry on the upper troposphere. Stratospheric ozone changes (10.3 DU ppm$(CH_4)^{-1}$) are twice as large as the tropospheric changes, but still small compared to the total stratospheric column. We find that stratospheric water vapor produced by oxidation of methane causes small decreases in stratospheric ozone (–4.3 DU ppm$(CH_4)^{-1}$).

Ozone generally has greater radiative forcing efficiency in the troposphere than in the stratosphere (Forster and Shine, 1997), so tropospheric ozone changes tend to dominate the ozone RF components. In our 3 models, tropospheric ozone RF is 30-50% of the direct methane RF, and up to 65% after including stratospheric ozone mediated by methane and water. Previous IPCC assessments have assumed 25% for purposes of calculating GWP (Forster et al., 2007; Shine et al., 1995), similar to a recent estimate of 21% based on tropospheric changes alone (Fry et al., 2012). Methane perturbation data from the TAR (3.67 DU(O_3) ppm$(CH_4)^{-1}$) (Prather et al., 2001), however, suggest that tropospheric ozone RF is about 40% of the methane RF (154 mW m^{-2} ppm$(CH_4)^{-1}$, assuming efficiency of 42 mW m^{-2} DU$(O_3)^{-1}$) (Ramaswamy et al., 2001).

Accounting for both direct and indirect effects, the methane RF efficiency, F_e, is 618 mW m^{-2} ppm$(CH_4)^{-1}$ in steady-state. A 1 Tg pulse emission of methane raises the atmospheric abundance by $\delta = 0.364$ ppb, which decays at a rate $f\,\tau_{CH4}$, where $f = 1.33$ is the methane feedback on its lifetime. We use $\tau_{CH4} = 9.14$ y (Prather et al., 2012). Neglecting delays between emission time and stratospheric impacts, the 100-y absolute GWP is $\delta\, f\, \tau_{CH4}\, F_e = 2.75$ mW a m^{-2}, compared to 0.087 mW a m^{-2} for CO_2. Thus, the methane GWP_{100} is 31.6. Our result is higher than several previous reports, generally near 25 (Forster et al., 2007; Fry et al., 2012), mainly because we include stratospheric ozone effects, but also because the updated and longer methane lifetime used here

(Prather et al., 2012). IPCC TAR recommended $f = 1.4$ (Prather et al., 2001), which would imply an even larger GWP, but since f depends on τ_{CH4} the two must be chosen consistently. Uncertainty in the GWP is difficult to assess without further modeling and analysis of stratospheric impacts, but it is likely ±20% or larger.

4 Historical (1980-2005) changes in CH_4 lifetime

Having established the ability of Equation 1 to reconstruct $\tau_{CH4\times OH}$ over 1997-2009 in CTMs, we now use it to extrapolate methane lifetime over several decades for which the CTMs have not been run. We begin with the historical period 1980-2005, during which time the key atmospheric forcing variables have been relatively well observed by satellites and ground stations.

In addition to the 5 climate and emission variables identified in Section 3.2 as important influences on interannual variability, we include CH_4 abundance and anthropogenic NOx emissions from land, ships, and aircraft for the historical reconstruction. We also include sensitivity to anthropogenic CO and VOC emissions, based on the IPCC TAR parameters, but without uncertainties (Prather et al., 2001). In total, the expanded parametric model includes 11 parameters and variables. For the sensitivity parameters, α_i in Equation 1, we adopt values from the average and spread of sensitivities in the 3 CTMs (Table 2, last column).

Table 3 summarizes the data sources for historical climate and emission variables in the expanded parametric model. NASA MERRA reanalysis provides temperature and water vapor data (Bosilovich et al., 2011) and satellite observations provide ozone column data (Stolarski and Frith, 2006). As with the 5-parameter model, these are averaged over the latitudes, 40°S to 40°N, that are important for CH_4 oxidation. Historical CH_4 abundance and anthopogenic and biomass burning emissions follow CMIP5 recommendations (Lamarque et al., 2010; Meinshausen et al., 2011b). Global annual lightning flash rates have varied by up to 20% since 1998, but multi-decadal trends are not apparent (Murray et al., n.d.), so we assume no change since 1980, with 10% Gaussian uncertainty in the trend.

Figure 5 shows the historical changes in $\tau_{CH4\times OH}$ reconstructed from Equation 1, together with the contribution from each of the climate and emission variables. To account for uncertainties in parameters and the lightning forcing, we generate 10^5 monte carlo realizations of Equation 1, allowing all parameters to vary independently. The resulting uncertainty in the $\tau_{CH4\times OH}$ reconstruction, measured as standard deviation across the realizations, reflects uncertainty in the

parameters, α_i, but not uncertainty in emissions, ozone observation, or meteorological assimilation. (See Figure S6 for uncertainties in $\tau_{CH4\times OH}$ in each component.)

Our reconstruction has annual variability of 1-2 % in $\tau_{CH4\times OH}$ over the 1980-2005 period. Reductions in $\tau_{CH4\times OH}$ occur during El Niño years—1982-3, 1987-8, and 1997-8—driven mainly by water vapor and reinforced by a smaller effect from temperature. Stratospheric ozone changes, forced by the solar cycle and Mt. Pinatubo, depresses $\tau_{CH4\times OH}$ through much of the 1990s. The largest spikes in $\tau_{CH4\times OH}$ occur when the solar cycle maximum and La Niña are synchronous, as in 1989 and 1999-2000. Overall, the parametric model simulates a decrease in $\tau_{CH4\times OH}$ since 1980, which has also been found in numerous CTM and GCM studies (Dentener et al., 2003; Duncan et al., 2000; Hess and Mahowald, 2009; Karlsdottir and Isaksen, 2000; Naik et al., n.d.; Stevenson et al., 2005). This is an improvement over previous parametric approaches, which are shown in Figure 5, that produce zero or positive trends over the same period (Meinshausen et al., 2011a; Prather et al., 2001).

Figure 6 identifies the contribution of each variable to the total change in $\tau_{CH4\times OH}$. Rising atmospheric methane has the largest influence on $\tau_{CH4\times OH}$, but the positive methane feedback effect (4%) is more than compensated by negative climate and emission terms. Temperature and water vapor, which have increased due to GHGs, decrease $\tau_{CH4\times OH}$ by 2%, collectively, although the water vapor effect is about 3 times larger. Halogen-driven decreases in stratospheric ozone also shortened the lifetime about 1%. Increases in ship and land anthropogenic NOx emissions both decrease $\tau_{CH4\times OH}$ by 1.5%, despite the ship source have much smaller total magnitude. Lightning NOx could also have an important impact on $\tau_{CH4\times OH}$, but the lightning trends are not known.

The total $\tau_{CH4\times OH}$ change from 1980-5 to 2000-5 is 2.3 ± 1.8 % in our model, or 0.13 % a^{-1} from a linear fit. Dentener et al. (2003), simulated a larger decrease, –0.2 % a^{-1}, in the 1980s that they attributed mainly to water vapor. Meteorological inputs may contribute to the difference, since water vapor trends are known to vary amongst reanalysis products (Trenberth et al., 2011). In addition, the shift of anthropogenic emissions to SE Asia, which alters the sensitivity of $\tau_{CH4\times OH}$ to emissions is not treated in the parametric model (e.g. Fuglestvedt et al., 1999; Karlsdottir and Isaksen, 2000). Methyl chloroform analyses generally suggest large decreases in $\tau_{CH4\times OH}$ during the 1980s followed by increases during the 1990s, which conflicts with the CTM results (Bousquet et al., 2005; Prinn et al., 2005). Assuming uncertainty of about 20% in methyl

chloroform emissions, however, reconciles the observations with the small trends found in CTMs and in our parametric model (Krol and Lelieveld, 2003; Prinn et al., 2005).

5 Future (2010-2100) CH_4 and CH_4 lifetime

We now apply the parametric model to predict methane and methane lifetime, with their uncertainties, following a future socioeconomic scenario. We make predictions for RCP 8.5 (Riahi et al., 2007), a scenario with rapid climate warming, but these methods apply to other scenarios as well. The prediction begins with the best estimate of present-day (2010) methane budget, including natural and anthropogenic emissions, and lifetimes for all loss processes, using the method of Prather et al. (2012). The scenario specifies future anthropogenic methane emissions and we assume natural emissions could change ±20% (1σ) by 2100. We use the parametric model to predict future $\tau_{CH4\times OH}$ and adopt other loss rates from literature (Prather et al., 2012). For future predictions we use the same expanded set of 11 parameters as were used in the historical $\tau_{CH4\times OH}$ reconstruction (Table 2, last column). Table 3 lists data sources for the future climate and emission variables.

Table 4 summarizes the predicted changes in climate and emissions in RCP 8.5. In this scenario most anthropogenic emissions of ozone precursors decrease by 2100 (7-75%), although aircraft NOx emissions rise 123%. Biomass burning emissions, also specified by the scenario, decrease 35%. The parametric prediction requires tropospheric temperature and water vapor inputs consistent with the scenario, but averages over the relevant latitudes (40°S–40°N) and altitudes (surface to 400 hPa) are not readily available, so we calculate them from sea-surface temperature (SST) in CMIP5 models that have simulated RCP 8.5 (Climate Explorer, http://climexp.knmi.nl/, accessed July 18, 2012). Regressions between annual-mean SST and both temperature and water vapor are derived from reanalysis data since 1979, and these relations are used to predict future temperature and water vapor from the simulated SST. Uncertainties are propagated from the SST range in CMIP5 ensemble and from present-day regression fitting errors (See Table 4 footnotes and Supplement for details). In 2100, we calculate tropospheric temperature and water vapor to be 3.7 ± 0.9 K and 38.2 ± 8.9 % larger than 2010, respectively. For tropical stratospheric ozone, multiple models predict recovery to 1980 levels around 2045 due to the decrease of long-lived halogenated gases (Austin and Scinocca, 2010; Eyring et al., 2010a; Newman et al., 2007), followed by GHG-driven decreases through 2100 (Eyring et al., 2010a). We adopt this projection, adding uncertainty that grows to 3% of the total column in 2100. Lightning NOx emissions have been estimated in past work to grow 5–50% by the late 21st century (Wu et al., 2008), but these

predictions are highly speculative due to poor mechanistic understanding of present-day global flash rates. GHG-driven climate warming tends to reduce convection (Held and Soden, 2006), but may intensify convection in some regions (Del Genio et al., 2007), so the total effect on lightning is unclear. In this work we assume 10% increase by 2100, but allow broad Gaussian uncertainty of 20%. As in our earlier work, we account for uncertainties in parametric terms, climate variables, and the present-day budget with 10^5 monte carlo realizations of future methane in RCP 8.5 (Prather et al., 2012).

Figure 6 shows future methane and its uncertainty through 2100. Projected abundances reach 3950 ± 320 ppb in 2100, which is about 500 ppb lower than our previous work (Prather et al., 2012), which did not account for emissions and climate controls on $\tau_{CH4\times OH}$. MAGICC predicts lower concentrations, 3750 ppb, due mainly to the strong negative sensitivity of $\tau_{CH4\times OH}$ to temperature in that model, but the MAGICC values lie within our estimated uncertainties throughout the 21st century. Statistical uncertainties in methane predictions are 8% in 2100, based on the assessed processes in the parametric model. Neglected processes—including shifting emission locations, biogenic VOC emissions, stratosphere-troposphere exchange, and aerosol interactions with photolysis and chemistry—might cause additional systematic prediction errors, but we have found that these have minor impact on present-day interannual $\tau_{CH4\times OH}$ variability.

The parametric model predicts $\tau_{CH4\times OH}$ will increase +13.3 ± 10.0 % by 2100 (Figure 6). MAGICC gives similar results (+12.6 %), but the IPCC TAR formula yields a larger result (+29.6 %), consistent with their respective historical performances in Section 4. The ACCMIP model ensemble predicts +6.2 ± 10.2 % for RCP 8.5 (Voulgarakis et al., n.d.), which demonstrates that the simple parametric approach covers much of the range suggested by computationally intensive GCM ensemble integrations. Lightning NOx emissions likely explain most of the $\tau_{CH4\times OH}$ difference, since ACCMIP models calculate 24 % increase in 2100 (Voulgarakis et al., n.d.). Although we do not think future lightning estimates from GCMs are robust (see above), assuming an equally large change in the parametric model would lower $\tau_{CH4\times OH}$ in 2100 by more than 4%, after accounting for methane feedback.

Figure 7 and Table 4 decompose the net $\tau_{CH4\times OH}$ changes in 2050 into components due to each climate and emission variable. Uncertainties here include possible errors in both the sensitivity and forcing variable, except for the emission terms where all uncertainty comes from the sensitivity parameter. Methane feedback is the largest influence, having an individual contribution of +29.0 ± 7.3 %. NOx emission reductions over land also force $\tau_{CH4\times OH}$ upwards

(+12.8 ± 0.9%), which is opposite to NOx influence in recent decades. Other climate and emission components are zero or negative, with water vapor having the largest effect (–11.5 ± 2.8 %). Stratospheric ozone and lightning NOx contribute little to $\tau_{CH4\times OH}$ changes, but they make a significant contribution to the uncertainty.

6 Conclusions

Over 1997-2009, the 3 CTMs in this work exhibit common variability in methane lifetime, which is also shared by other published model studies. We quantitatively explain these features with 5 climate and emission variables—temperature, water vapor, ozone column, biomass burning emissions, lightning NOx emissions. A parametric model built on these 5 factors reproduces 50-90% of the variability in methane lifetime during 1997-2009. The ensemble of 3 models provides a measure of uncertainty in each parametric factor, which we use to project past and future methane and its lifetime, with uncertainties. While this approach lacks the full complexity of atmospheric chemistry that can be included through multi-decadal simulations of a CTM or GCM, the advantage is that it can be rapidly applied to many climate data sets or socioeconomic scenarios. Using the parametric model to reconstruct methane lifetime for 1980-2005, we estimate 2.3±1.8% decrease in $\tau_{CH4\times OH}$, which is the same direction of change as previous CTM studies but smaller magnitude. For the RCP 8.5 future scenario, methane abundances are larger than the CMIP5 recommendations, which are based on the MAGICC model, but the uncertainty encompasses the difference. Uncertainty in 2100 abundance is 10% based on the processes we have assessed here. Water vapor, anthropogenic NOx emissions, and methane feedback on its OH sink are the major drivers of $\tau_{CH4\times OH}$ in both the historical and future simulations.

We also provide a new estimate of the indirect components of methane RF. Tropospheric ozone contributes 30-50% of the direct methane RF, compared to 25% that has been used in previous IPCC assessments (Forster et al., 2007). After including stratospheric chemistry effects, including those mediated by water vapor, we estimate the methane-induced ozone RF to be 50% of the direct methane RF. Based on these data, the 100-year methane GWP is 32.

Acknowledgments

We thank Mingquan Mu (UC Irvine) for providing additional GEOS-Chem simulations that we compare to our results. This research was supported by the NASA Modeling, Analysis, and Prediction Program (NNX09AJ47G), the Office of Science (BER) of the U.S. Department of Energy (DE-SC0007021), and the Kavli Chair in Earth System Science.

References

Austin, J. and Scinocca, J.: Long-term projections of stratospheric ozone, in SPARC Report on the Evaluation of Chemistry-Climate Models, vol. SPARC Report No. 5, WCRP-132, edited by V. Eyring, T. G. Shepherd, and D. W. Waugh, WMO. 2010.

Bian, H., Prather, M. and Takemura, T.: Tropospheric aerosol impacts on trace gas budgets through photolysis, J Geophys Res-Atmos, 108(D8), 4242, doi:10.1029/2002JD002743, 2003.

Bosilovich, M. G., Robertson, F. R. and Chen, J.: Global Energy and Water Budgets in MERRA, J Climate, 24(22), 5721–5739, doi:10.1175/2011JCLI4175.1, 2011.

Bousquet, P., Hauglustaine, D., Peylin, P., Carouge, C. and Ciais, P.: Two decades of OH variability as inferred by an inversion of atmospheric transport and chemistry of methyl chloroform, Atmospheric Chemistry And Physics, 5, 2635–2656, 2005.

Carver, G., Brown, P. and Wild, O.: The ASAD atmospheric chemistry integration package and chemical reaction database, Comput Phys Commun, 105, 197–215, 1997.

Chen, G., Huey, L., Trainer, M., Nicks, D., Corbett, J., Ryerson, T., Parrish, D., Neuman, J., Nowak, J., Tanner, D., Holloway, J., et al.: An investigation of the chemistry of ship emission plumes during ITCT 2002, J Geophys Res-Atmos, 110, –, doi:10.1029/2004JD005236, 2005.

Christian, H., Blakeslee, R., Boccippio, D., Boeck, W., Buechler, D., Driscoll, K., Goodman, S., Hall, J., Koshak, W., Mach, D. and Stewart, M.: Global frequency and distribution of lightning as observed from space by the Optical Transient Detector, J Geophys Res-Atmos, 108, –, doi:10.1029/2002JD002347, 2003.

Dalsoren, S. B., Eide, M. S., Myhre, G., Endresen, O., Isaksen, I. S. A. and Fuglestvedt, J. S.: Impacts of the Large Increase in International Ship Traffic 2000-2007 on Tropospheric Ozone and Methane, Environ Sci Technol, 44(7), 2482–2489, doi:10.1021/es902628e, 2010.

Del Genio, A. D., Yao, M.-S. and Jonas, J.: Will moist convection be stronger in a warmer climate? Geophys Res Lett, 34(16), L16703, doi:10.1029/2007GL030525, 2007.

Dentener, F., Peters, W., Krol, M., van Weele, M., Bergamaschi, P. and Lelieveld, J.: Interannual variability and trend of CH4 lifetime as a measure for OH changes in the 1979-1993 time period, J Geophys Res-Atmos, 108(D15), 4442, doi:10.1029/2002JD002916, 2003.

Dlugokencky, E. J., Nisbet, E. G., Fisher, R. and Lowry, D.: Global atmospheric methane: budget, changes and dangers, Philos T R Soc A, 369(1943), 2058–2072, doi:10.1098/rsta.2010.0341, 2011.

Duncan, B. N., Bey, I., Chin, M., Mickley, L. J., Fairlie, T. D., Martin, R. V. and Matsueda, H.: Indonesian wildfires of 1997: Impact on tropospheric chemistry, J Geophys Res-Atmos, 108, 4458, doi:10.1029/2002JD003195, 2003.

Duncan, B., Portman, D., Bey, I. and Spivakovsky, C.: Parameterization of OH for efficient computation in chemical tracer models, J Geophys Res-Atmos, 105, 12259–12262, 2000.

Eyring, V., Cionni, I., Lamarque, J. F., Akiyoshi, H., Bodeker, G. E., Charlton-Perez, A. J., Frith,

S. M., Gettelman, A., Kinnison, D. E., Nakamura, T., Oman, L. D., et al.: Sensitivity of 21st century stratospheric ozone to greenhouse gas scenarios, Geophys Res Lett, 37, L16807, doi:10.1029/2010GL044443, 2010a.

Eyring, V., Isaksen, I. S. A., Berntsen, T., Collins, W. J., Corbett, J. J., Endresen, O., Grainger, R. G., Moldanova, J., Schlager, H. and Stevenson, D. S.: Transport impacts on atmosphere and climate: Shipping, Atmos Environ, 44(37), 4735–4771, doi:10.1016/j.atmosenv.2009.04.059, 2010b.

Fiore, A. M., Dentener, F. J., Wild, O., Cuvelier, C., Schultz, M. G., Hess, P., Textor, C., Schulz, M., Doherty, R. M., Horowitz, L. W., MacKenzie, I. A., et al.: Multimodel estimates of intercontinental source-receptor relationships for ozone pollution, J Geophys Res-Atmos, 114, –, doi:10.1029/2008JD010816, 2009.

Fiore, A. M., Horowitz, L. W., Dlugokencky, E. J. and West, J. J.: Impact of meteorology and emissions on methane trends, 1990-2004, Geophys Res Lett, vol.33, no.12, 4 pp., doi:10.1029/2006GL026199, 2006.

Fiore, A. M., West, J. J., Horowitz, L. W., Naik, V. and Schwarzkopf, M. D.: Characterizing the tropospheric ozone response to methane emission controls and the benefits to climate and air quality, Journal of Geophysical Research - Part D - Atmospheres, D08307 (16 pp.), doi:10.1029/2007JD009162, 2008a.

Fiore, A. M., West, J. J., Horowitz, L. W., Naik, V. and Schwarzkopf, M. D.: Characterizing the tropospheric ozone response to methane emission controls and the benefits to climate and air quality, J Geophys Res-Atmos, 113(D8), D08307, doi:10.1029/2007JD009162, 2008b.

Forster, P. and Shine, K. P.: Radiative forcing and temperature trends from stratospheric ozone changes, J Geophys Res-Atmos, 102, 10841–10855, 1997.

Forster, P., Ramaswamy, V., Artaxo, P., Berntsen, T., Betts, R., Fahey, D. W., Haywood, J., Lean, J., Lowe, D., Myhre, G., Nganga, J., et al.: Changes in Atmospheric Constituents and in Radiative Forcing, in Climate Change 2007: The Physical Science Basis. Contribution of Working Group I to the Fourth Assessment Report of the Intergovernmental Panel on Climate Change, edited by S. Solomon, D. Qin, M. Manning, Z. Chen, M. Marquis, K. Averyt, M. Tignor, and H. Miller, Cambridge University Press, Cambridge. 2007.

Fry, M. M., Naik, V., West, J. J., Schwarzkopf, M. D., Fiore, A. M., Collins, W. J., Dentener, F. J., Shindell, D. T., Atherton, C., Bergmann, D., Duncan, B. N., et al.: The influence of ozone precursor emissions from four world regions on tropospheric composition and radiative climate forcing, J Geophys Res-Atmos, 117, –, doi:10.1029/2011JD017134, 2012.

Fuglestvedt, J., Berntsen, T., Isaksen, I., Mao, H., Liang, X. and Wang, W.: Climatic forcing of nitrogen oxides through changes in tropospheric ozone and methane; global 3D model studies, Atmos Environ, 33(6), 961–977, 1999.

Granier, C., Bessagnet, B., Bond, T., D'Angiola, A., van der Gon, H. D., Frost, G. J., Heil, A., Kaiser, J. W., Kinne, S., Klimont, Z., Kloster, S., et al.: Evolution of anthropogenic and biomass burning emissions of air pollutants at global and regional scales during the 1980-2010 period, Climatic Change, 109, 163–190, doi:10.1007/s10584-011-0154-1, 2011.

606 Guenther, A., Karl, T., Harley, P., Wiedinmyer, C., Palmer, P. I. and Geron, C.: Estimates of
607 global terrestrial isoprene emissions using MEGAN (Model of Emissions of Gases and Aerosols
608 from Nature), Atmospheric Chemistry And Physics, 6, 3181–3210, 2006.

609 Held, I. M. and Soden, B. J.: Robust responses of the hydrological cycle to global warming, J
610 Climate, 19(21), 5686–5699, 2006.

611 Hess, P. and Mahowald, N.: Interannual variability in hindcasts of atmospheric chemistry: the
612 role of meteorology, Atmospheric Chemistry And Physics, 9(14), 5261–5280, 2009.

613 Holmes, C. D., Tang, Q. and Prather, M. J.: Uncertainties in climate assessment for the case of
614 aviation NO, P Natl Acad Sci Usa, 108(27), 10997–11002, doi:10.1073/pnas.1101458108, 2011.

615 Hoor, P., Borken-Kleefeld, J., Caro, D., Dessens, O., Endresen, O., Gauss, M., Grewe, V.,
616 Hauglustaine, D., Isaksen, I. S. A., Jockel, P., Lelieveld, J., et al.: The impact of traffic emissions
617 on atmospheric ozone and OH: results from QUANTIFY, Atmospheric Chemistry And Physics,
618 9(9), 3113–3136, 2009.

619 Hsu, J. and Prather, M. J.: Stratospheric variability and tropospheric ozone, J Geophys Res-
620 Atmos, 114, D06102, doi:10.1029/2008JD010942, 2009.

621 IPCC: Climate Change 2007: The Physical Science Basis. Contribution of Working Group I to
622 the Fourth Assessment Report of the Intergovernmental Panel on Climate Change, edited by S.
623 Solomon, D. Qin, M. Manning, Z. Chen, M. Marquis, K. Averyt, M. Tignor, and H. Miller,
624 Cambridge University Press, Cambridge, UK. 2007.

625 Isaksen, I., Zerefos, C., Kourtidis, K., Meleti, C., Dalsoren, S., Sundet, J., Grini, A., Zanis, P. and
626 Balis, D.: Tropospheric ozone changes at unpolluted and semipolluted regions induced by
627 stratospheric ozone changes, J Geophys Res-Atmos, 110(D2), D02302,
628 doi:10.1029/2004JD004618, 2005.

629 Jacob, D., Field, B., Jin, E., Bey, I., Li, Q., Logan, J. and Yantosca, R.: Atmospheric budget of
630 acetone, J. Geophys. Res., 107, 4100, 2002.

631 Karlsdottir, S. and Isaksen, I.: Changing methane lifetime: Possible cause for reduced growth,
632 Geophys Res Lett, 27(1), 93–96, 2000.

633 Krol, M. and Lelieveld, J.: Can the variability in tropospheric OH be deduced from measurements
634 of 1,1,1-trichloroethane (methyl chloroform)? J Geophys Res-Atmos, 108(D3), 4125,
635 doi:10.1029/2002JD002423, 2003.

636 Lamarque, J. F., Bond, T. C., Eyring, V., Granier, C., Heil, A., Klimont, Z., Lee, D., Liousse, C.,
637 Mieville, A., Owen, B., Schultz, M. G., et al.: Historical (1850-2000) gridded anthropogenic and
638 biomass burning emissions of reactive gases and aerosols: methodology and application,
639 Atmospheric Chemistry And Physics, 10(15), 7017–7039, doi:10.5194/acp-10-7017-2010, 2010.

640 Lamarque, J. F., Shindell, D., Josse, B., Eyring, V., Young, P. J., Cionni, I., Bergmann, D.,
641 Cameron-Smith, P., Collins, W. J., Doherty, R., Dalsoren, S. B., et al.: The Atmospheric
642 Chemistry and Climate Model Intercomparison Project (ACCMIP): Overview and description of
643 models, simulations and climate diagnostics, Geosci. Model Dev. Discuss., in review, n.d.

644 Lamarque, J.-F., Kyle, G. P., Meinshausen, M., Riahi, K., Smith, S. J., van Vuuren, D. P.,
645 Conley, A. J. and Vitt, F.: Global and regional evolution of short-lived radiatively-active gases
646 and aerosols in the Representative Concentration Pathways, Climatic Change, 109, 191–212,
647 doi:10.1007/s10584-011-0155-0, 2011.

648 Lawrence, M. G. and Salzmann, M.: On interpreting studies of tracer transport by deep cumulus
649 convection and its effects on atmospheric chemistry, Atmospheric Chemistry And Physics, 8(20),
650 6037–6050, 2008.

651 Lee, D. S., Pitari, G., Grewe, V., Gierens, K., Penner, J. E., Petzold, A., Prather, M. J., Schumann,
652 U., Bais, A., Berntsen, T., Iachetti, D., et al.: Transport impacts on atmosphere and climate:
653 Aviation, Atmos Environ, 44(37), 4678–4734, doi:10.1016/j.atmosenv.2009.06.005, 2010.

654 Lelieveld, J. and Crutzen, P.: Role of Deep Cloud Convection in the Ozone Budget of the
655 Troposphere, Science, 264(5166), 1759–1761, 1994.

656 Macintyre, H. L. and Evans, M. J.: Sensitivity of a global model to the uptake of N2O5 by
657 tropospheric aerosol, Atmospheric Chemistry And Physics, 10(15), 7409–7414, doi:10.5194/acp-
658 10-7409-2010, 2010.

659 Mao, J., Jacob, D. J., Evans, M. J., Olson, J. R., Ren, X., Brune, W. H., St Clair, J. M., Crounse,
660 J. D., Spencer, K. M., Beaver, M. R., Wennberg, P. O., et al.: Chemistry of hydrogen oxide
661 radicals (HOx) in the Arctic troposphere in spring, Atmospheric Chemistry And Physics, 10(13),
662 5823–5838, doi:10.5194/acp-10-5823-2010, 2010.

663 Martin, R., Jacob, D., Yantosca, R., Chin, M. and Ginoux, P.: Global and regional decreases in
664 tropospheric oxidants from photochemical effects of aerosols, J Geophys Res-Atmos, 108(D3),
665 4097, doi:10.1029/2002JD002622, 2003.

666 McCulloch, A., Aucott, M., Graedel, T., Kleiman, G., Midgley, P. and Li, Y.: Industrial
667 emissions of trichloroethene, tetrachloroethene, and dichloromethane: Reactive Chlorine
668 Emissions Inventory, J Geophys Res-Atmos, 104(D7), 8417–8427, 1999.

669 Meinshausen, M., Raper, S. C. B. and Wigley, T. M. L.: Emulating coupled atmosphere-ocean
670 and carbon cycle models with a simpler model, MAGICC6-Part 1: Model description and
671 calibration, Atmospheric Chemistry And Physics, 11(4), 1417–1456, doi:10.5194/acp-11-1417-
672 2011, 2011a.

673 Meinshausen, M., Smith, S. J., Calvin, K., Daniel, J. S., Kainuma, M. L. T., Lamarque, J. F.,
674 Matsumoto, K., Montzka, S. A., Raper, S. C. B., Riahi, K., Thomson, A., et al.: The RCP
675 greenhouse gas concentrations and their extensions from 1765 to 2300, Climatic Change, 109,
676 213–241, doi:10.1007/s10584-011-0156-z, 2011b.

677 Millet, D. B., Guenther, A., Siegel, D. A., Nelson, N. B., Singh, H. B., de Gouw, J. A., Warneke,
678 C., Williams, J., Eerdekens, G., Sinha, V., Karl, T., et al.: Global atmospheric budget of
679 acetaldehyde: 3-D model analysis and constraints from in-situ and satellite observations,
680 Atmospheric Chemistry And Physics, 10(7), 3405–3425, doi:10.5194/acp-10-3405-2010, 2010.

681 Montzka, S. A., Krol, M., Dlugokencky, E., Hall, B., Joeckel, P. and Lelieveld, J.: Small
682 Interannual Variability of Global Atmospheric Hydroxyl, Science, 331(6013), –,
683 doi:10.1126/science.1197640, 2011.

684 Murray, L. T., Jacob, D. J., Logan, J. A., Hudman, R. C. and Koshak, W. J.: Optimized regional
685 and interannual variability of lightning in a global chemical transport model constrained by
686 LIS/OTD satellite data, J. Geophys. Res., in review, n.d.

687 Myhre, G., Nilsen, J. S., Gulstad, L., Shine, K. P., Rognerud, B. and Isaksen, I. S. A.: Radiative
688 forcing due to stratospheric water vapour from CH4 oxidation, Geophys Res Lett, 34(1), L01807,
689 doi:10.1029/2006GL027472, 2007.

690 Myhre, G., Shine, K. P., Raedel, G., Gauss, M., Isaksen, I. S. A., Tang, Q., Prather, M. J.,
691 Williams, J. E., van Velthoven, P., Dessens, O., Koffi, B., et al.: Radiative forcing due to changes
692 in ozone and methane caused by the transport sector, Atmos Environ, 45(2), 387–394,
693 doi:10.1016/j.atmosenv.2010.10.001, 2011.

694 Naik, V., Voulgarakis, A., Fiore, A. M., Lamarque, J. F., Lin, M., Prather, M. J., Young, P. J.,
695 Bergmann, D., Cameron-Smith, P. J., Cionni, I., Collins, W. J., et al.: Preindustrial to present day
696 changes in tropospheric hydroxyl radical and methane lifetime from the Atmospheric Chemistry
697 Climate Model Intercomparison Project (ACCMIP), in preparation, n.d.

698 Neu, J. L., Prather, M. J. and Penner, J. E.: Global atmospheric chemistry: Integrating over
699 fractional cloud cover, J Geophys Res-Atmos, 112(D11), D11306, doi:10.1029/2006JD008007,
700 2007.

701 Newman, P. A., Daniel, J. S., Waugh, D. W. and Nash, E. R.: A new formulation of equivalent
702 effective stratospheric chlorine (EESC), Atmospheric Chemistry And Physics, 7(17), 4537–4552,
703 2007.

704 Olson, J., Crawford, J., Chen, G., Brune, W., Faloona, I., Tan, D., Harder, H. and Martinez, M.: A
705 reevaluation of airborne HOx observations from NASA field campaigns, J Geophys Res-Atmos,
706 111, –, doi:10.1029/2005JD006617, 2006.

707 Ott, L. E., Pickering, K. E., Stenchikov, G. L., Allen, D. J., DeCaria, A. J., Ridley, B., Lin, R.-F.,
708 Lang, S. and Tao, W.-K.: Production of lightning NOx and its vertical distribution calculated
709 from three-dimensional cloud-scale chemical transport model simulations, J Geophys Res-Atmos,
710 115, D04301, doi:10.1029/2009JD011880, 2010.

711 Prather, M.: Numerical Advection by Conservation of 2nd-Order Moments, J Geophys Res-
712 Atmos, 91, 6671–6681, 1986.

713 Prather, M. J., Zhua, X., Strahan, S. E., Steenrod, S. D. and Rodriguez, J. M.: Quantifying errors
714 in trace species transport modeling, P Natl Acad Sci Usa, 105(50), 19617–19621,
715 doi:10.1073/pnas.0806541106, 2008.

716 Prather, M., Ehhalt, D., Dentener, F., Derwent, R., Dlugokencky, E., Holland, E., Isaksen, I.,
717 Katima, J., Kirchhoff, V., Matson, P., Midgley, P., et al.: Atmospheric Chemistry and Greenhouse
718 Gases, in Climate Change 2001: The Scientific Basis. Third Assessment Report of the
719 Intergovernmental Panel on Climate Change, edited by J. Houghton, Y. Ding, D. Griggs, M.
720 Noguer, P. van der Linden, X. Dai, K. Maskell, and C. Johnson, Cambridge University Press,
721 Cambridge, UK. 2001.

722 Prather, M., Holmes, C. and Hsu, J.: Reactive greenhouse gas scenarios: Systematic exploration
723 of uncertainties and the role of atmospheric chemistry, Geophys Res Lett, 39,

724 doi:10.1029/2012GL051440, 2012.

725 Price, C. and Rind, D.: Modeling global lightning distributions in a general circulation model,
726 Mon Weather Rev, 122(8), 1930–1939, 1994.

727 Prinn, R., Huang, J., Weiss, R., Cunnold, D., Fraser, P., Simmonds, P., McCulloch, A., Harth, C.,
728 Reimann, S., Salameh, P., O'Doherty, S., et al.: Evidence for variability of atmospheric hydroxyl
729 radicals over the past quarter century, Geophys Res Lett, 32(7), L07809,
730 doi:10.1029/2004GL022228, 2005.

731 Ramaswamy, V., Boucher, O., Haigh, J., Hauglustaine, D., Haywood, J., Myhre, G., Nakajima,
732 T., Shi, G. Y. and Solomon, S.: Radiative Forcing of Climate Change, in Cliamte Change 2001:
733 The Scientific Basis. Third Assessment Report of the Intergovernmental Panel on Climate
734 Change, edited by J. T. Houghton, Y. Ding, D. Griggs, M. Noguer, P. J. van der Linden, X. Dai,
735 K. Maskell, and C. Johnson, Cambridge University Press, Cambridge, UK. 2001.

736 Riahi, K., Grübler, A. and Nakicenovic, N.: Scenarios of long-term socio-economic and
737 environmental development under climate stabilization, Technological Forecasting and Social
738 Change, 74, 887–935, 2007.

739 Rienecker, M. M., Suarez, M. J., Gelaro, R., Todling, R., Bacmeister, J., Liu, E., Bosilovich, M.
740 G., Schubert, S. D., Takacs, L., Kim, G.-K., Bloom, S., et al.: MERRA: NASA's Modern-Era
741 Retrospective Analysis for Research and Applications, J Climate, 24(14), 3624–3648,
742 doi:10.1175/JCLI-D-11-00015.1, 2011.

743 Rienecker, M. M., Suarez, M. J., Todling, R., Bacmeister, J., Takacs, L., Liu, H.-C., Gu, W.,
744 Sienkiewicz, M., Koster, R. D., Gelaro, R., Stajner, I., et al.: The GEOS-5 Data Assimilation
745 System, Technical Report Series on Global Modeling and Data Assimilation. 2008.

746 Sauvage, B., Martin, R. V., van Donkelaar, A., Liu, X., Chance, K., Jaegle, L., Palmer, P. I., Wu,
747 S. and Fu, T. M.: Remote sensed and in situ constraints on processes affecting tropical
748 tropospheric ozone, Atmospheric Chemistry And Physics, 7, 815–838, 2007.

749 Schultz, M. G., Heil, A., Hoelzemann, J. J., Spessa, A., Thonicke, K., Goldammer, J. G., Held, A.
750 C., Pereira, J. M. C. and van het Bolscher, M.: Global wildland fire emissions from 1960 to 2000,
751 Global Biogeochem. Cycles, 22(2), GB2002, doi:10.1029/2007GB003031, 2008.

752 Shine, K. P., Fouquart, Y., Ramaswamy, V., Solomon, S. and Srinivasan, J.: Radiative Forcing, in
753 Climate Change 1994: Radiative Forcing of Climate Change and An Evaluation of the IPCC IS92
754 Emission Scenarios. Reports of Working Groups I and III of the Intergovernmental Panel of
755 Climate Change, edited by J. Houghton, L. Meira Filho, J. Bruce, H. Lee, B. Callander, E. Haites,
756 N. Harris, and K. Maskell, Cambridge University Press, Cambridge. 1995.

757 Stevenson, D., Doherty, R., Sanderson, M., Johnson, C., Collins, B. and Derwent, D.: Impacts of
758 climate change and variability on tropospheric ozone and its precursors, Faraday Discuss, 130,
759 41–57, doi:10.1039/b417412g, 2005.

760 Stolarski, R. S. and Frith, S. M.: Search for evidence of trend slow-down in the long-term
761 TOMS/SBUV total ozone data record: the importance of instrument drift uncertainty,
762 Atmospheric Chemistry And Physics, 6, 4057–4065, 2006.

763 Søvde, O. A., Prather, M. J., Isaksen, I. S. A., Berntsen, T. K., Stordal, F., Zhu, X., Holmes, C. D.
764 and Hsu, J.: The chemical transport model Oslo CTM3, Geosci. Model Dev. Discuss., 5(2),
765 1561–1626, doi:10.5194/gmdd-5-1561-2012, 2012.

766 Tang, Q. and Prather, M. J.: Correlating tropospheric column ozone with tropopause folds: the
767 Aura-OMI satellite data, Atmospheric Chemistry And Physics, 10(19), 9681–9688,
768 doi:10.5194/acp-10-9681-2010, 2010.

769 Tiedtke, M.: A Comprehensive Mass Flux Scheme for Cumulus Parameterization in Large-Scale
770 Models, Mon Weather Rev, 117(8), 1779–1800, 1989.

771 Trenberth, K. E., Fasullo, J. T. and Mackaro, J.: Atmospheric Moisture Transports from Ocean to
772 Land and Global Energy Flows in Reanalyses, J Climate, 24(18), 4907–4924,
773 doi:10.1175/2011JCLI4171.1, 2011.

774 van der Werf, G. R., Randerson, J. T., Giglio, L., Collatz, G. J., Mu, M., Kasibhatla, P. S.,
775 Morton, D. C., DeFries, R. S., Jin, Y. and van Leeuwen, T. T.: Global fire emissions and the
776 contribution of deforestation, savanna, forest, agricultural, and peat fires (1997-2009),
777 Atmospheric Chemistry And Physics, 10(23), 11707–11735, doi:10.5194/acp-10-11707-2010,
778 2010.

779 van Vuuren, D. P., Edmonds, J., Kainuma, M., Riahi, K., Thomson, A., Hibbard, K., Hurtt, G. C.,
780 Kram, T., Krey, V., Lamarque, J.-F., Masui, T., et al.: The representative concentration pathways:
781 an overview, Climatic Change, 109, 5–31, doi:10.1007/s10584-011-0148-z, 2011.

782 Vinken, G. C. M., Boersma, K. F., Jacob, D. J. and Meijer, E. W.: Accounting for non-linear
783 chemistry of ship plumes in the GEOS-Chem global chemistry transport model, Atmospheric
784 Chemistry And Physics, 11(22), 11707–11722, doi:10.5194/acp-11-11707-2011, 2011.

785 Volk, C., Elkins, J., Fahey, D., Dutton, G., Gilligan, J., Loewenstein, M., Podolske, J., CHAN, K.
786 and Gunson, M.: Evaluation of source gas lifetimes from stratospheric observations, J Geophys
787 Res-Atmos, 102(D21), 25543–25564, 1997.

788 Voulgarakis, A., Naik, V., Lamarque, J.-F., Shindell, D. T., Prather, M. J., Wild, O., Young, P. J.,
789 Bergmann, D., Cameron-Smith, P., Cionni, I., Collins, W. J., et al.: Multimodel simulations of
790 present-day and future OH and methane lifetime, Atmospheric Chemistry And Physics
791 Discussions, in review, n.d.

792 Voulgarakis, A., Savage, N. H., Wild, O., Braesicke, P., Young, P. J., Carver, G. D. and Pyle, J.
793 A.: Interannual variability of tropospheric composition: the influence of changes in emissions,
794 meteorology and clouds, Atmospheric Chemistry And Physics, 10(5), 2491–2506,
795 doi:10.5194/acp-10-2491-2010, 2010.

796 Wang, J. S., McElroy, M. B., Logan, J. A., Palmer, P. I., Chameides, W. L., Wang, Y. and
797 Megretskaia, I. A.: A quantitative assessment of uncertainties affecting estimates of global mean
798 OH derived from methyl chloroform observations, J Geophys Res-Atmos, 113(D12), D12302,
799 doi:10.1029/2007JD008496, 2008.

800 Wennberg, P., Peacock, S., Randerson, J. and Bleck, R.: Recent changes in the air-sea gas
801 exchange of methyl chloroform, Geophys Res Lett, 31(16), L16112, doi:10.1029/2004GL020476,
802 2004.

803 Wu, S., Mickley, L. J., Jacob, D. J., Rind, D. and Streets, D. G.: Effects of 2000-2050 changes in
804 climate and emissions on global tropospheric ozone and the policy-relevant background surface
805 ozone in the United States, J Geophys Res-Atmos, 113(D18), D18312,
806 doi:10.1029/2007JD009639, 2008.

807 Yamaguchi, K. and Noda, A.: Global warming patterns over the North Pacific: ENSO versus AO,
808 J Meteorol Soc Jpn, 84(1), 221–241, 2006.

809

810

Tables

Table 1. Emissions

Source (Inventory)[a]	NOx, Tg(N) a^{-1}	CO, Tg a^{-1}	Isoprene, Tg a^{-1}
Anthropogenic (RCP year 2000)	32[b]	609	-
Biomass burning (GFED3)	5.6[c]	360[c]	-
Biogenic (MEGAN)	-	76	523
Lightning	5[d]	-	-
Total	42	1047	523

[a] Inventory references: RCP (Lamarque et al., 2011), GFED3 (van der Werf et al., 2010), MEGAN (Guenther et al., 2006).

[b] Land, ship, and aviation components are 26, 5.4, and 0.85 Tg(N) a^{-1}, respectively.

[c] Average biomass burning for 1997-2009. Emissions for individual years are 3.3-6.1 Tg(N) a^{-1} and 263-605 Tg(CO) a^{-1}.

[d] Average for 1997-2009 in UCI CTM and Oslo CTM3. Emissions for individual years are 4.8-5.4 Tg(N) a^{-1}. GEOS-Chem has 5.7-6.4 Tg(N) a^{-1} (average 6 Tg(N) a^{-1}) over 2004-2009.

Table 2. Sensitivity of $\tau_{CH_4 \times OH}$ to climate variables and emissions [a]

Variable	UCI CTM	Oslo CTM3	GEOS-Chem	Literature [g]	Adopted [f]
Chemistry-climate interactions					
Air temperature*†[b]	–3.9	–2.8	–2.2		–3.0 ± 0.8
Water vapor*†[b]	–0.32	–0.29	–0.34		–0.32 ± 0.03
Ozone column*†[e]	+0.66	+0.43	+0.61	+0.28-0.76 [7]	+0.55 ± 0.11
Lightning NOx emissions*†	–0.14	–0.11	–0.24		–0.16 ± 0.06
Biomass burning emissions*†[c]	+0.021	+0.024	+0.017		+0.021 ± 0.010
CH_4 abundance†[d]	+0.363	+0.307	+0.274	+0.32 [1] +0.28 ± 0.03 [2]	+0.31 ± 0.04 (f = 1.34 ± 0.06)
Convective mass flux	–0.036				N
Optical depth, ice clouds	+0.013				N
Optical depth, water clouds	–0.025				N
Anthropogenic emissions					
Land NOx†[h]	–0.15	–0.10	–0.16	–0.137 [1] –0.121±0.055 [3]	–0.14 ± 0.03
Ship NOx†	–0.045	–0.050	–0.017	–0.0412 ± 0.01 [4] –0.0374 ± 0.005 [5]	–0.03 ± 0.015
Aviation NOx†				–0.014 ± 0.003 [6]	–0.014 ± 0.003
CO†				0.11 [1] 0.074 ± 0.004 [3]	0.11
VOC†				0.047 [1] 0.033 ± 0.01 [3]	0.047

* Major cause of interannual $\tau_{CH4 \times OH}$ variability, used for $\tau_{CH4 \times OH}$ reconstruction in Section 3.

† Used for 1980-2100 prediction of $\tau_{CH4 \times OH}$ in Sections 4 and 5.

[a] Sensitivities are $d\ln(\tau_{CH4 \times OH})/d\ln(F)$ for each variable F. Values calculated for 1998-9 perturbations simulations in UCI CTM and Oslo CTM3 and 2004-5 for GEOS-Chem, except where noted below for biomass burning and CH_4 feedback. Perturbation magnitudes were chosen to be similar to interannual variability or decadal trend (see Table S1 for exact magnitudes).

[b] Tropospheric perturbation only.

[c] Biomass burning sensitivity in UCI CTM ranges over 0.008-0.046 (See Figure 3). Value for the UCI CTM is the emission-weighted average for 1997-2009. Values for other models are scaled to 1997-2009 means, assuming the same relative variability as the UCI CTM. Adopted uncertainty accounts for this large sensitivity changes between years.

[d] f is the methane feedback factor, defined as the ratio of methane perturbation lifetime to total budget lifetime (Prather et al., 2001). We calculate f using recent estimates of all methane sinks (Prather et al., 2012). Using IPCC TAR lifetimes increases f by 0.03.

[e] Ozone columns over 40°S-40°N are perturbed only in photolysis calculations. Responses in UCI CTM and GEOS-Chem are due solely to tropospheric chemistry. The Oslo CTM3 response

836 includes stratospheric chemistry and stratosphere-troposphere exchange, but CTM3 results are
837 rescaled to the same ozone perturbations as the other models.

838 [f] Adopted values are the mean of CTMs, except for CO, VOC, and aviation NOx, which come
839 from literature. Uncertainties are 1-σ values based on CTM spread and expert assessment. Terms
840 marked N have negligible impact on interannual $\tau_{CH4\times OH}$ variability and are not used in the
841 parametric model.

842 [g] [1] (Prather et al., 2001), [2] (Fiore et al., 2009), [3] (Fry et al., 2012), [4] (Hoor et al., 2009),
843 [5] (Myhre et al., 2011), [6] (Holmes et al., 2011) [7] (Karlsdottir and Isaksen, 2000)

844 [h] All anthropogenic emission occurring over land, including combustion, agriculture, and waste.

845

Table 3. Datasets for historical and future $\tau_{CH_4 \times OH}$

Variable	Dataset			
	Historical (1980-2005)	Source[a]	Future (2010-2100)	Source[a]
Temperature	MERRA	[1]	CMIP5[b]	[5]
Water vapor	MERRA	[1]	CMIP5[b]	[5]
Column O_3	TOMS/SBUV	[2]	SPARC	[6]
L-NOx	0 ± 10 %	Assumed	+10 ± 20 %	Assumed
Biomass burning	CMIP5	[3]	RCP 8.5	[7]
Anthropogenic emissions (NOx, CO, VOC)	CMIP5	[3]	RCP 8.5	[7]
CH_4 abundance	CMIP5	[4]	this work[c]	

[a] [1] (Bosilovich et al., 2011), [2] (Stolarski and Frith, 2006), [3] (Eyring et al., 2010b; Lamarque et al., 2010; Lee et al., 2010; Schultz et al., 2008), [4] CMIP5 historical GHG recommendations (Meinshausen et al., 2011b) [5] Ensemble of 34 CMIP5 models (Climate Explorer, http://climexp.knmi.nl/, accessed July 18, 2012) [6] CCM-Val2 multimodel mean for SRES A1B greenhouses gases and A2 ozone depleting substances (Austin and Scinocca, 2010; Eyring et al., 2010a), uncertainties assumed to be ± 3% in 2100. [7] (Riahi et al., 2007; van Vuuren et al., 2011)

[b] Future atmospheric temperature is calculated from sea-surface temperature (SST) in each CMIP5 model. Water vapor is then calculated from atmospheric temperature using standard vapor pressure formulas and assuming constant relative humidity. The range of SST in the CMIP5 models is propagated to uncertainty in air temperature and water vapor. See Supplement for details.

[c] We calculate future CH_4 using $\tau_{CH4 \times OH}$ from Equation 1 (adopted parameters from Table 2 and other inputs from this Table) and RCP 8.5 emissions of CH_4. Other sinks and natural emissions, plus their uncertainties, are from Prather et al. (2012). We also specify ±20% uncertainty in natural CH_4 emissions in 2100. Uncertatinties in all terms are propagated using the monte carlo approach of Prather et al.

Table 4. Changes (2100-2010) in climate variables, emissions, and $\tau_{CH_4 \times OH}$ for RCP 8.5[a]

Variable	Variable change	$\tau_{CH4 \times OH}$ change, %
Air temperature, 40°S-40°N[b]	+3.7 ± 0.9 K	-4.2 ± 1.5
Water vapor, 40°S-40°N	+38.5 ± 9.1 %	-11.5 ± 2.8
Ozone column, 40°S-40°N	0.7 ± 3.0 %	0.4 ± 1.7
Lightning NOx emissions	10 ± 20 %	-1.2 ± 3.3
Biomass burning emissions	-34.8 %	+0.9 ± 0.4
CH_4 abundance	+78.5 ± 7.9 %	+29.0 ± 7.3
Anthropogenic emissions		
Land NOx	-75.3 %	+12.8 ± 0.9
Ship NOx	-7.2 %	+0.2 ± 0.1
Aircraft NOx	+123 %	-1.7 ± 0.4
CO	-44.0 %	-4.7
VOC	-11.1 %	-0.5
Total (this work)		+13.3 ± 10.0
IPCC TAR Total (Prather et al., 2001)		+29.6
MAGICC Total (Meinshausen et al., 2011a)		+12.6

[a] Variable changes from data sources in Table 3, except CH_4 abundance, which is calculated from the scenario CH_4 emissions and the time-evolving $\tau_{CH4 \times OH}$ (see text). $\tau_{CH4 \times OH}$ component changes derived from the variable changes and the sensitivities in Table 2, including uncertainties in both.

[b] Surface to 400 hPa average.

Table 5. Present-day, steady-state methane impact on ozone and radiative forcing[a]

	UCI CTM	Oslo CTM3	GEOS-Chem	Literature	Adopted
Ozone chemistry, DU(O_3) ppm(CH_4)$^{-1}$					
d[O_3]/d[CH_4]	4.03(T)	4.98(T)	2.90(T)	3.5±1.0(T)[b] 3.0±0.8(T)[c]	
d[O_3]/d[H_2O] (from CH_4)		10.32(S) –0.40(T) –4.35(S)			
Radiative forcing, mW m^{-2} ppm(CH_4)$^{-1}$					
CH_4	367	367	367	370 ± 27[d]	370
O_3 from CH_4	141(T)	198(T) 78(S)	108(T)[f]	126 ± 45(T)[b]	150(T) 78(S)
O_3 from CH_4 via H_2O		–16(T) –19(S)			–16(T) –19(S)
H_2O from CH_4				55[e]	55
Total					618
100-year GWP				25[d] 24.2 ± 4.2[e]	31.6

[a] Troposphere (T) and stratosphere (S) values given separately, wherever possible. All CTM results are for 2009.

[b] (review by Holmes et al., 2011)

[c] (Fry et al., 2012)

[d] (Forster et al., 2007)

[e] 15% of CH_4 direct RF (Myhre et al., 2007)

[f] Calculated from tropospheric O_3 change using the average RF efficiency from the other models.

Figures

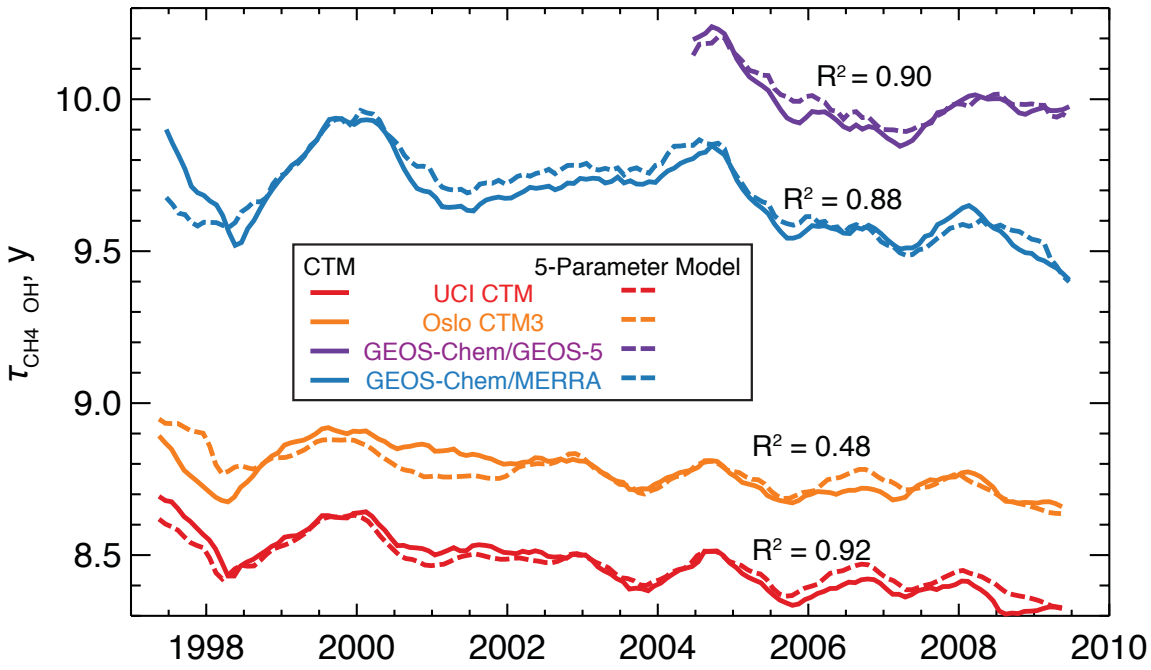

Figure 1.

Methane lifetime due to oxidation by tropospheric OH ($\tau_{CH4\times OH}$) simulated by each CTM (solid lines) and reconstructed from the 5-parameter model (dashed lines). The parameters are temperature, water vapor, ozone column, lightning NOx emission, and biomass burning emission. Parameter values for each CTM are given in Table 2 and the corresponding variables are in Figure 2. R^2 values show correlation between each CTM and its own 5-parameter model. GEOS-Chem simulations use either MERRA or GEOS-5 meteorology. All lifetimes are smoothed with a 12-month running mean.

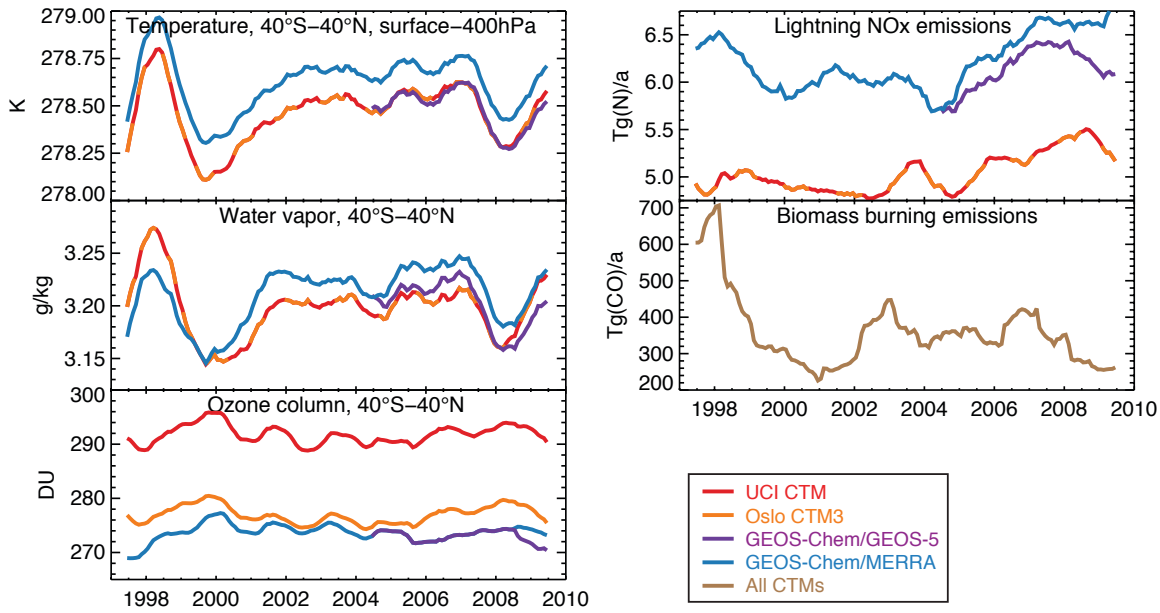

892

893 **Figure 2.**

894 Climate and emission variables controlling the interannual variation of $\tau_{CH4\times OH}$ in CTMs.
895 Emissions are global totals, while other climate variables are averaged over 40°S – 40°N, where
896 80 % of methane oxidation occurs. Colors indicate which inputs are used by each CTM.

897

898

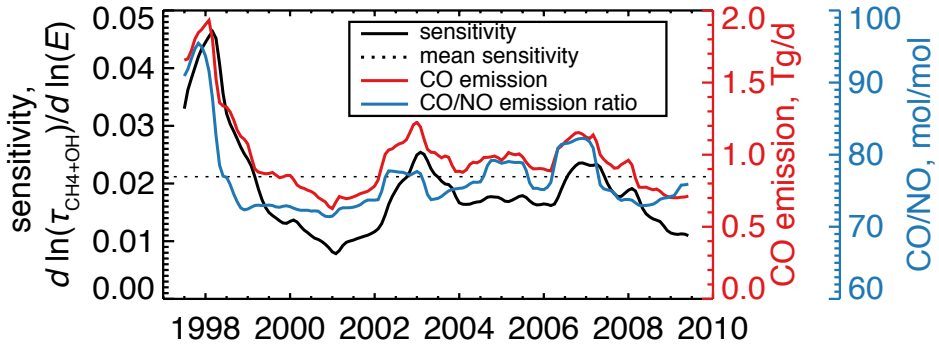

Figure 3.

Sensitivity of $\tau_{CH4\times OH}$ to biomass burning emissions, *E*, in the UCI CTM. Biomass burning CO emissions and the CO/NO emission ratio from the GFED3 inventory are also shown. Peak emissions and CO/NO ratio occur during El Niño events, due to tropical peat fires.

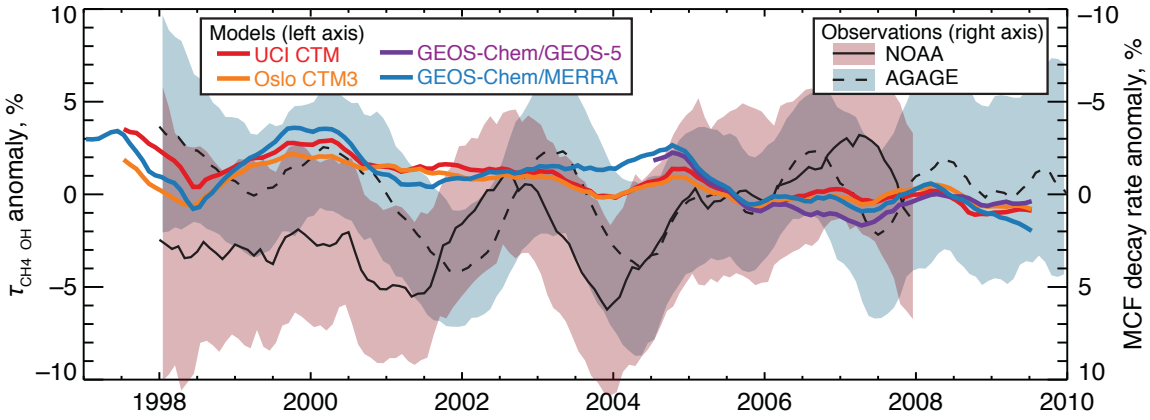

Figure 4.

Interannual variability of $\tau_{CH4\times OH}$ in CTMs and observed methyl chloroform (MCF) decay rate. Observations are derived from atmospheric MCF abundances at NOAA and AGAGE surface stations (Montzka et al., 2011; Prinn et al., 2005), with an uncertainty (shaded) given by the 16th to 84th percentile range (±1σ) of decay rates across stations within each network, and adjusted by the tropospheric OH fraction of total MCF loss. All data are shown as anomalies relative to their own 2004-2010 mean (2004-2008 for NOAA data). Models, observations, and uncertainties are smoothed with a 12-month running average. Note anomalies in $\tau_{CH4\times OH}$ and decay rate have opposite sign.

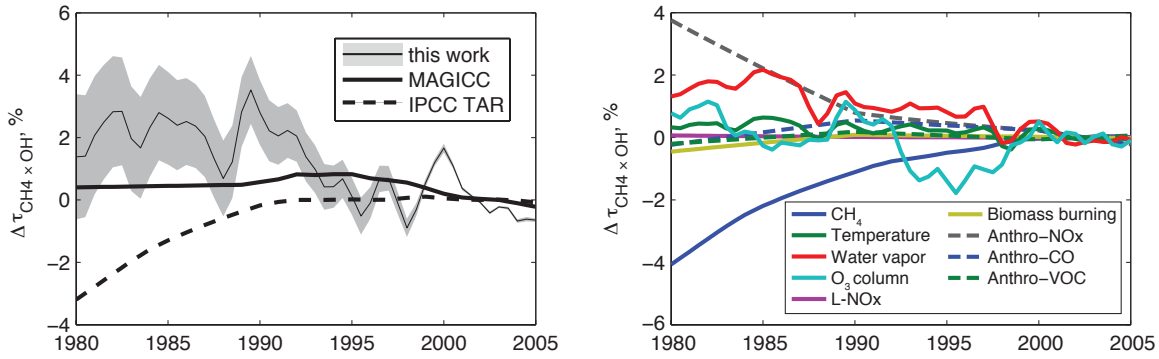

914

915 **Figure 5.**

916 Recent historical $\tau_{CH4\times OH}$ variation (left) and its component causes (right). Lifetime reconstructed
917 in this work from Eq. 1, with components shown at right. Shaded region shows ± σ uncertainty
918 propagated from parameter ranges in Table 2, but not including possible errors in reanalysis,
919 ozone, or emission inputs. All data are anomalies with respect to their 2000-2005 means. The
920 anthropogenic (anthro) NOx component combines the separate effects of land, ship, and aircraft
921 emissions. See Figure S6 for uncertainties in each component.

922

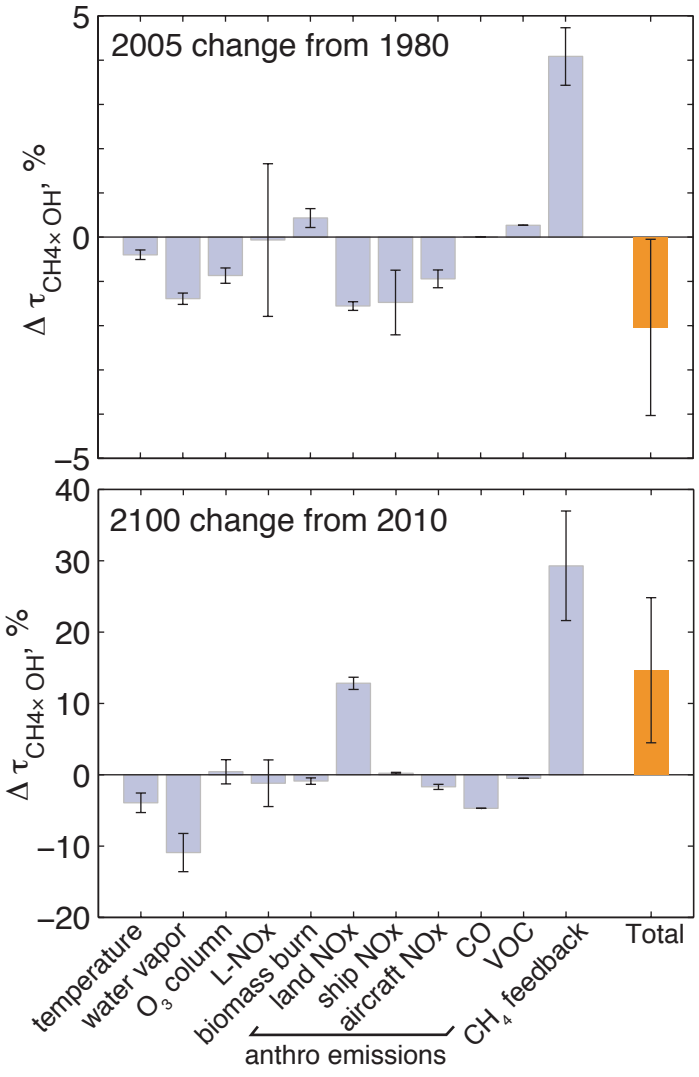

922

923 **Figure 6.**

924 Contribution of emissions and chemistry-climate interactions to changes in $\tau_{CH4\times OH}$ from 1980 to
925 2005 (top) and from 2010 to 2100 (bottom). Components and their uncertainties are derived from
926 parameters in Table 2 and forcing variables in Table 3. Uncertainties (vertical bars) are standard
927 deviations from 10^5 monte carlo integrations. Note the different vertical scales.

928

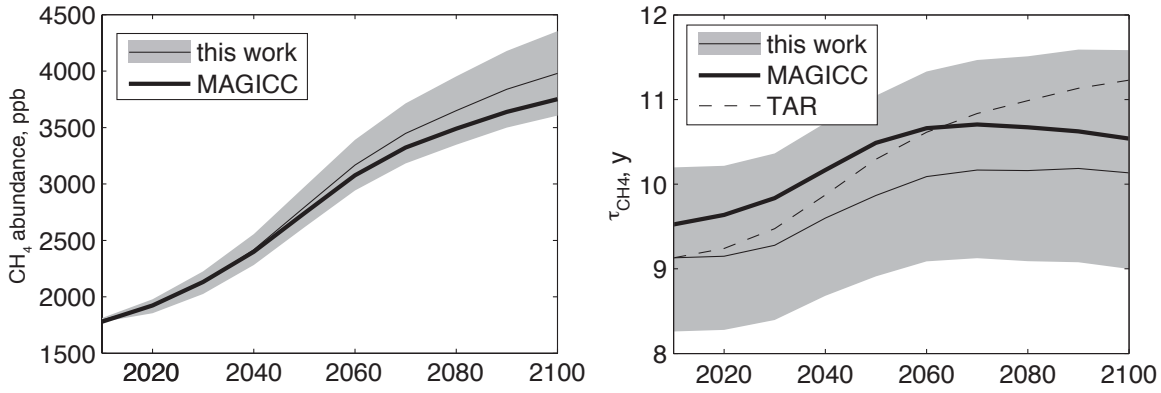

928

929 **Figure 7.**

930 Projected future methane abundance (left) and total lifetime (right) for RCP 8.5. Projected
931 uncertainty (shaded) is the standard deviation from 10^5 monte carlo integrations, accounting for
932 uncertainty in the present-day budget, emissions, and climate-chemistry effects on $\tau_{CH4\times OH}$. Our
933 projections are compared to MAGICC model (Meinshausen et al., 2011a) and the IPCC TAR
934 formula (Prather et al., 2001).

Supplementary Information:

Future methane, hydroxyl, and their uncertainties: key climate and emission parameters for future predictions

Christopher D. Holmes [1*], Michael J. Prather [1], Amund O. Søvde [2], Gunnar Myhre [2]

[1] Department of Earth System Science, University of California, Irvine, CA 92697-3100 USA

[2] Center for International Climate and Environmental Research (CICERO), Oslo, Norway

[*] Correspondence to cdholmes@uci.edu

Methyl chloroform decay rate and its uncertainty

The AGAGE network consists of 5 sites, each of which makes measurements every 20 minutes, with analysis and calibration done on site. In the NOAA network, flasks are filled 1-4 times monthly and analyzed in a central laboratory in Boulder, Colorado. To avoid pollution influences, flasks are filled when winds blow from a clean sector. In the AGAGE network polluted samples are identified as anomalously high MCF concentrations and removed from analysis.

Both networks provide monthly average data for each of their sites, which we use here (NOAA: (IPCC, 2007), accessed Jan 5, 2012; AGAGE: (Prather et al., 2001), accessed April 4, 2012). For the NOAA network, we use data from the same 9 sites as Montzka et al. (2011) (South Pole; Cape Grim, Australia; Cape Matatula, American Samoa; Alert, Canada; and United States sites at Mauna Loa, Hawaii; Niwot Ridge, Colorado; KLEF tower, Minnesota; and Barrow, Alaska). All 5 AGAGE sites are used here analysis (Cape Grim, Australia; Cape Matatula, American Samoa; Ragged Point, Barbados; Trinidad Head, United States; and Mace Head, Ireland). NOAA data are truncated at December 2007 due to later quality issues (S. Montzka, pers. comm.).

Our method for calculating the global MCF decay rate differs from that of Montzka et al. (2011). Montzka et al. first constructed a global mean tropospheric MCF abundance from a weighted average of the sites, then calculated the global decay rate using the same formula we have applied to each site individually. We find our method to be much less sensitive to site selection and methods for filling missing data, but our global mean decay rates and their anomalies are, nevertheless, very similar, as shown in Figure S1. Differences are always less than 1% after 2000, but are as large as 2% in early 1998, due to more frequent data gaps in the early period.

Future tropospheric temperature and water vapor

The parametric model for $\tau_{CH4\times OH}$ requires atmospheric temperature and water vapor as inputs, averaged over 40°S-40°N and from the surface to 400 hPa. These input data must be consistent with other scenario emission data, which are taken from RCP 8.5 in this work. Averages over the required region, where 80% of methane oxidation occurs, are not readily available from CMIP5

models. Therefore, for our future methane predictions, we derive atmospheric temperature and water vapor from sea-surface temperature (SST) in the CMIP5, using historical correlations between these climate variables.

Figure S3 shows strong correlations between historical (1979-2010) SST and tropospheric temperatures for the region of fast methane loss. These correlations are robust against different meteorological analysis products (R^2=0.7 to 0.8). Using MERRA data (Bosilovich et al., 2011) since 1979, the slope of atmosphere vs. sea-surface temperatures is 1.28 ± 0.1. ECMWF data (cycle 36r1, (Prather et al., 2012)) since 1997 yield a statistically indistinguishable value. Using other SST data (e.g. Reynolds et al., 2002) does not alter the result (not shown). A slope greater than 1 is expected from physical princples and Santer et al. (2005) found a similar ratio of 1:1.3 for multidecadal trends in surface temperature vs. lower tropospheric temperature.

Water vapor mixing ratio can be calculated from atmospheric temperature using standard vapor pressure formulas (e.g. Eq. 2.61 Jacobson, 2005), assuming constant relative humidity. Figure S4 shows that the calculated water vapor is highly correlated with reanalysis water vapor (R^2 = 0.7-0.8) with a slope of 1.51 ± 0.18 when the calculations are based on SST. The slope deviates from 1:1 because both temperature and water vapor are averaged over a large region (40°S-40°N, surface to 400 hPa), while vapor pressure formulas strictly apply only to homogeneous regions.

An ensemble of 34 CMIP5 models provide SST predictions for RCP 8.5 climate (Climate Explorer, http://climexp.knmi.nl/, accessed July 18, 2012). We calculate future atmospheric temperature, $T_i(t)$ in each model i to be

$$T_i(t) = T_0 * [1 + a_1 * (SST_i(t) / SST_i(t_0) - 1)],$$

Where $SST_i(t)$ is the model's SST, t_0 = 2010, T_0 = 278.5 K (ECMWF 2000-2009 mean), and a_1 = N(1.3, 0.1) is a normally distributed random number that accounts for uncertainty in the historical fit between atmospheric temperature and SST. Future water vapor mixing ratio, $q_i(t)$, in the same model is

$$q_i(t) = p(T_0) + a_2 * [p(T_i(t)) - p(T_0)],$$

where $p(T)$ is the saturation vapor pressure at temperature T and a_2 = N(1.5, 0.2) accounts for uncertainty in the historical fit between water vapor and its SST-derived estimate. Through 10^5 monte carlo realizations of a_1 and a_2 we estimate uncertainty in atmospheric future temperature and water vapor in RCP 8.5.

Figure S5 shows the air temperature and water vapor changes inferred from the SST data. While SST increases 3.2 ± 0.6 K by 2100 in RCP 8.5, atmospheric temperatures increase 4.0 ± 0.9 K and water vapor increases 38.2 ± 8.9 % over the same period.

References

Bosilovich, M. G., Robertson, F. R. and Chen, J.: Global Energy and Water Budgets in MERRA, J Climate, 24(22), 5721–5739, doi:10.1175/2011JCLI4175.1, 2011.

Jacobson, M. Z.: Fundamentals of Atmospheric Modeling, 2nd ed. Cambridge University Press, Cambridge, UK. 2005.

Montzka, S. A., Krol, M., Dlugokencky, E., Hall, B., Joeckel, P. and Lelieveld, J.: Small Interannual Variability of Global Atmospheric Hydroxyl, Science, 331(6013), –, doi:10.1126/science.1197640, 2011.

88 Reynolds, R., Rayner, N., Smith, T., Stokes, D. and Wang, W.: An improved in situ and satellite
89 SST analysis for climate, J Climate, 15(13), 1609–1625, 2002.

90 Santer, B., Wigley, T., Mears, C., Wentz, F., Klein, S., Seidel, D., Taylor, K., Thorne, P.,
91 Wehner, M., Gleckler, P., Boyle, J., et al.: Amplification of surface temperature trends and
92 variability in the tropical atmosphere, Science, 309(5740), 1551–1556,
93 doi:10.1126/science.1114867, 2005.

94

95

96

Table S1: CTM simulations[a]

Description or perturbed variable	Perturbation		
	Magnitude	Region	Duration, y
Control simulation, no perturbations	-	-	UCI, CTM3: 13 GEOS-Chem MERRA: 13 GEOS-5: 6
Air temperature in chemistry solver	+1 K	global[c]	3
Water vapor in chemistry solver	+5 %	global[c]	3
Ozone column in photolysis code	+1 %	40°S-40°N	3
Biomass burning emissions	+5 %	global	3 (13 for UCI)
Lightning NOx emissions	+20 %	global	3
Anthropogenic NOx emissions over land	+7.8 %[b]	global	3
Anthropogenic NOx emissions from ships	+14.4%[b]	global	3
CH_4 abundance	+5 %	global	13
Convective mass flux	–20 %	global	3 (UCI only)
Cloud optical depth (all clouds) in photolysis code	+5 %	global	3 (UCI only)
Cloud optical depth (ice clouds) in photolysis code	+5 %	global	3 (UCI only)
Cloud optical depth (liquid clouds) in photolysis code	+5 %	global	3 (UCI only)

[a] Each variable is perturbed in a separate simulation. All perturbation tests are compared against a control run from the same CTM. GEOS-Chem perturbation tests use GEOS-5 meteorology only.
[b] This magnitude is the projected increase during the period 2000-2030 in RCP 8.5.
[c] In Oslo CTM3, temperature and water vapor perturbations are applied only to grid levels below 200 hPa to avoid confounding effects on stratospheric chemistry.

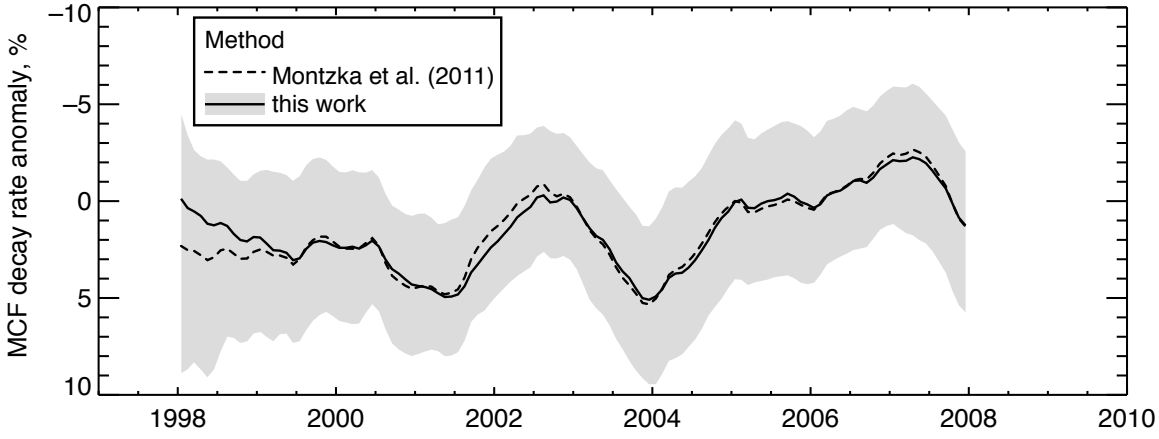

Figure S1. Global decay rate anomalies for methyl chloroform, calculated from NOAA data using two methods. Results from this work are compared to previously published work of Montzka et al. (2011). Shading shows the uncertainty, given by the 16th to 84th percentile range of decay rates across stations within each network, calculated in this work.

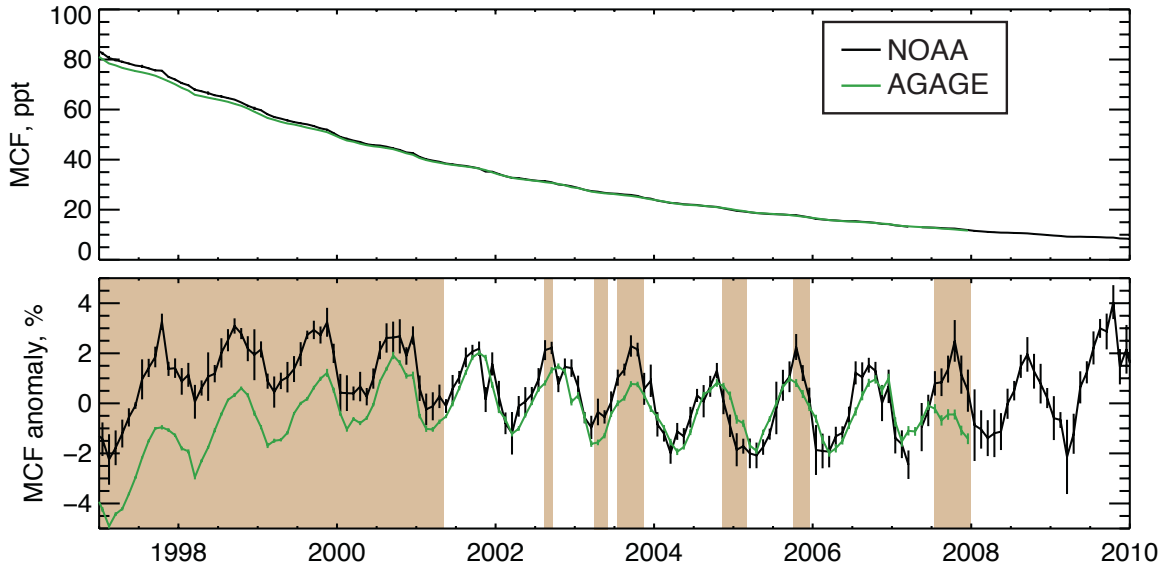

Figure S2. Methyl chloroform (MCF) abundance at the Cape Grim, Australia, as measured by the NOAA and AGAGE stations. Anomalies (bottom) are calculated with respect to a single decaying exponential reference curve that is fitted to all observations from both stations after 2000. Vertical lines show standard errors in the monthly mean abundances. Shading highlights episodes were the NOAA and AGAGE monthly means differ by more than their standard errors for 2 or more consecutive months.

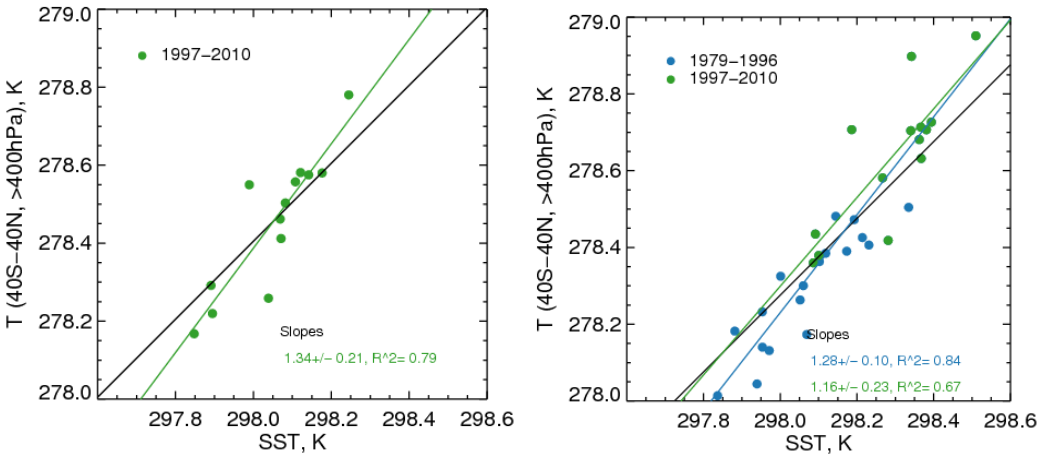

Figure S3. Annual mean tropospheric temperature in the region of rapid methane loss (40°S-40°N, surface to 400hPa) and annual mean SST (40°S-40°N) for ECMWF (left) and MERRA (right) meteorological analyses. Black line shows 1:1 relation. Blue and green lines are ordinary least squares regressions for all years and 1997-2010, respectively.

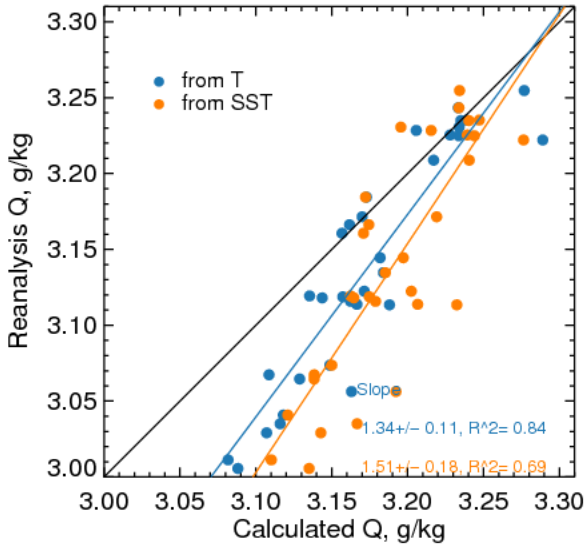

Figure S4. Water vapor mixing ratio from MERRA reanalysis (1979-2009) and calculated from temperature. Calculations are based on either SST (orange dots) or atmospheric temperature (blue dots) from MERRA reanalysis, using standard vapor pressure formulas, assuming constant relative humidity. Water vapor and SST are averaged over 40°S-40°N. Atmospheric temperatures are additionally averaged from the surface to 400hPa.

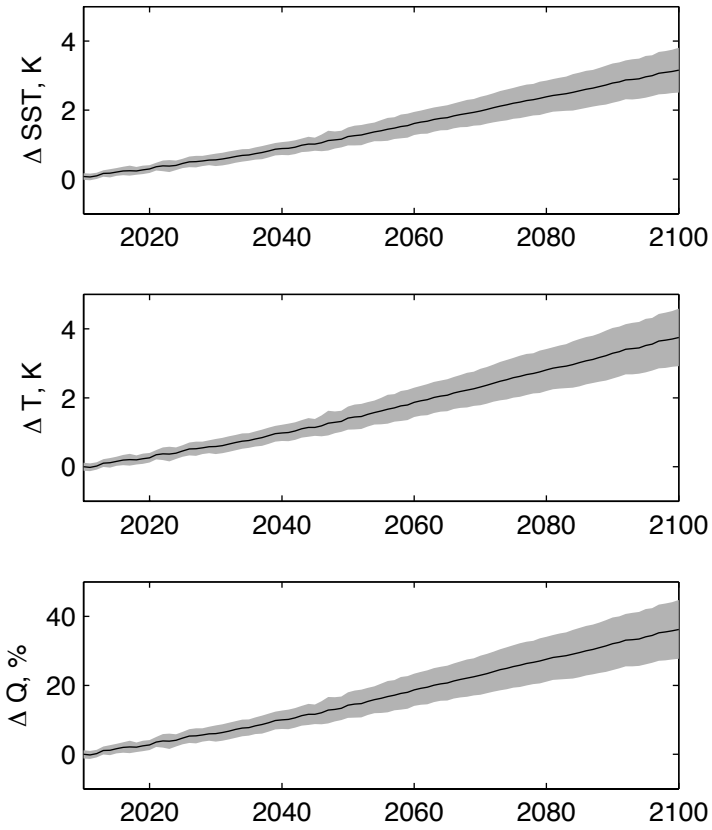

Figure S5. Predicted anomalies in SST (top), atmospheric temperature (middle), and water vapor (bottom) for RCP 8.5. SSTs are from an ensemble of 34 CMIP5 models, while other variables are derived from SSTs, as described in this supplement. All variables are averages over 40°S-40°N and atmospheric data are averaged from the surface to 400 hPa. Shading shows 1σ uncertainty.

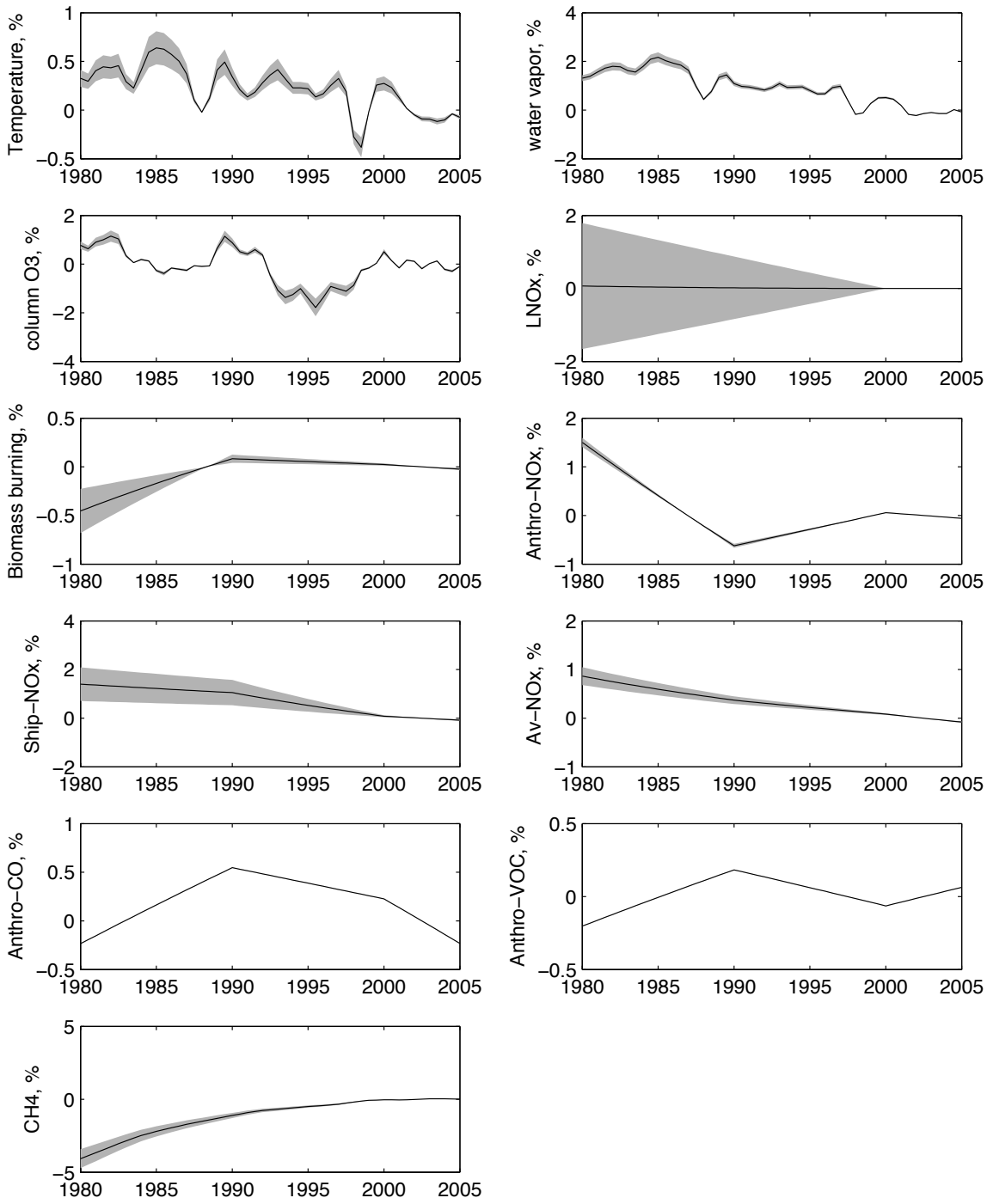

Figure S6. Contributions of climate and emission forcing variables to changes in $\tau_{CH4\times OH}$ since 1980. The sum of all contributions equals the change in lifetime shown in Figure 4.